Generalized Neural Mass Model Analysis and Applications Over Electroencephalogram Data

Sepehr Radmannia

A Thesis
in
The Department
of
Electrical and Computer Engineering

Presented in Partial Fulfillment of The Requirements
for The Degree of
Master of Applied Science (Electrical and Computer Engineering)
Concordia University
Montréal, Québec, Canada

April 2021

© Sepehr Radmannia, 2021

CONCORDIA UNIVERSITY
SCHOOL OF GRADUATE STUDIES

This is to certify that the thesis prepared

By: Sepehr Radmannia

Entitled: Generalized Neural Mass Model Analysis and Applications Over Electroencephalogram Data

and submitted in partial fulfillment of the requirements for the degree of

Master of Applied Science (Electrical and Computer Engineering)

complies with the regulations of this University and meets the accepted standards with respect to originality and quality.

Signed by the final examining committee:

_____ Chair
Dr. Omair Ahmad

_____ Examiner
Dr. Arash Mohammadi

_____ Examiner
Dr. Alexandre Vidal

_____ Supervisor
Dr. Habib Benali

_____ Co-supervisor
Dr. Hassan Rivaz

Approved by: _____
Dr. Wei-Ping Zhu, Chair
Department of Electrical and Computer Engineering

_____ 20___

_____
Dr. Mourad Debbabi, Dean,
Faculty of Engineering and Computer Science

Abstract

Generalized Neural Mass Model Analysis and Applications Over Electroencephalogram Data

Sepehr Radmannia

Computational modeling studies and explains neuronal behaviors by modeling their underlying dynamics. Specifically, Neural Mass Model (NMM) is a part of computational modeling that refers to populations (masses) of neurons inside the brain. NMMs have a variety of applications, e.g., characterization of the neurobiological process and artificial brain. NMMs are well investigated, and the available NMMs in the literature proposed two populations of neurons in communication with each other, namely, the population of pyramidal cells and the population of intra-neurons. Recent advanced technologies that facilitate spatiotemporal resolution neuroimaging data have contributed to develop more realistic NMMs. NMM's underlying behavioral dynamics must be appropriately analyzed to understand the brain's functional and structural relationship. In this thesis, first, we develop a novel method capable of detecting the model's underlying behavioral dynamics over high dimensional parameter space. This novel idea attempts to overcome the disadvantages of the bifurcation analysis over high-dimensional space. Moreover, physiologically interesting and non-interesting dynamics are localized over high-dimensional parameter space using the proposed approach. In order to validate the presented algorithm, we use the accuracy and F1-score as our metric. Second, we develop a method that localizes epileptic changes of electroencephalogram (EEG) signal over time as an application of NMMs in the real EEG data. It is studied in the state of the art that the gradual changes over the EEG signals can be interpreted as instability over the parameters of the NMMs. Furthermore, the progressive evolution of EEG's activity in pathological cases (e.g., epileptic seizures) is supposed to be characterized by a transition of the dynamics of the NMMs. The proposed algorithm is capable of detecting transitions of dynamics over simulated multi-dynamical signals. In addition, this method is capable of detecting the dynamic results in the best fitting time series with respect to frequency.

To my Parents

Acknowledgments

I want to express my deep appreciation to my supervisors Dr. Habib Benali and Dr. Hassan Rivaz, for their invaluable guidance and support throughout my master's degree. Without their continuous help and intuitive ideas, this thesis would not be possible. It was an honor to work with such knowledgeable and understanding supervisors.

I would like to thank my colleague for their great supports during this period. I had the opportunity to work with two research groups that allowed me to work in a healthy and enjoyable workspace with their support and kindly help.

I sincerely appreciate my supervisors, Concordia University, and Perform Centre research institutions for the financial support for this research study, which plays an important role in completing the research work. I wish to thank my friends at Concordia University: Mohsen Ghaderi, Ehsan Agah, and Kian Gheitasi, which they made this period the most memorable time in my life.

Last but not least, I really want to thank my beloved parents and my sister for their unconditional love and inspiration throughout my life. None of this would have been possible without their encouragement.

Contents

List of Figures

List of Tables

List of Symbols

A:	Average excitatory synaptic gain
B:	Average inhibitory synaptic gain
$\frac{1}{a}$:	Time constant of excitatory postsynaptic potentials
$\frac{1}{b}$:	Time constant of inhibitory postsynaptic potentials
e_0:	Half of the maximum discharge rate of a neuronal population
v_0:	Basic excitability threshold for neurons
r:	Stiffness of neuronal excitability
C_1:	Strength of the synaptic connections from P to P'
C_2:	Strength of the synaptic connections from P' to P
C_3:	Strength of the synaptic connections from P to I
C_4:	Strength of the synaptic connections from I to P
C:	Maximum number of synapses between populations
G:	Gain of the direct excitatory feedback from P to itself
P:	Main population of neurons
P':	Secondary population of neurons
I:	Inhibitory population of neurons

List of Abbreviations

NMM:	Neural Mass Model
GNMM:	Generalized Neural Mass Model
EEG:	Electroencephalogram
SVM:	Support Vector Machine
LDA:	Linear Discriminant Analysis
QDA:	Quadratic Discriminant Analysis
DT:	Decision Tree
LFP:	Local Field Potential
SEEG:	Stereo Electroencephalography
SN:	Saddle Node
NMO:	Noise Modulated Oscillations
NIS:	Noise Induced Spiking
NIS-OTO:	Noise Induced Spiking and Over Threshold Oscillations
NIS-STO:	Noise Induced Spiking and Subthreshold Oscillations
NITAM:	Noise Induced Thresholded Amplitude Modulation
ASM:	Attribute Selection Measure

Chapter 1

Introduction

The Neural Mass Modeling (NMM) field of study helps us understand the relationship between the brain's functional and structural connectivities by developing the brain's computational models. In Figure 1 two applications of NMM, e.g., characterization of the neurobiological process, the artificial brain, are shown. Recent advanced technology that facilitates spatiotemporal resolution neuroimaging data has contributed to developing more realistic models. NMM's underlying behavioral dynamics must be appropriately analyzed to understand the brain's functional and structural relationship.

To have a realistic brain model, the proposed neural mass model has to be built based on the physiologically meaningful hypothesis. For principal cells' excitatory feedback, two approaches have been considered in the literature. Direct feedback from the primary neural mass (Wilson andCowan (1973)) [1] or indirect feedback using an intermediate excitatory population (Jansen Rit, 1995; Jansen, Zouridakis, 1993) [2] Figure 2. Modeling point of view cannot give any privilege to one feedback over another. Local excitatory feedback (direct link) and distant excitatory feedback (indirect link) physiologically exist. Therefore, we used the NMM, proposed in [3]. The proposed NMM we used considers both direct and indirect excitatory feedback.

To analyze the NMM's underlying behavior, methods to deal with behavioral dynamics of the NMM over parameter space are needed. Bifurcation theory is one of the techniques

that has been used to analyze the NMMs underlying dynamics [3]. Nevertheless, proposed techniques only considering the limited number of parameters to analyze, and the other parameters are considered to be determined based on their literature values. The above statements motivate this thesis's first work, where novel detection and localization approach is provided to identify underlying behavior over high-dimensional parameter space.

NMMs were developed to simulate real electroencephalogram signals for understanding the brain's functional and structural relationship. The first step for this purpose is to develop a method proficient in detecting underlying dynamics from generated time series. The gradual changes over the Electroencephalogram (EEG) signal's physiological activities, can be interpreted as instability over parameters of the Neural Mass Model (NMM). The progressive evolution of EEG activity in pathological cases (e.g., epileptic seizures) is supposed to be characterized by a transition of the dynamics of the MNM. The above hypothesis motivates the thesis's second work, where we characterized each dynamics of the model to develop a new technique that identifies underlying behavioral dynamics from the simulated EEG time series.

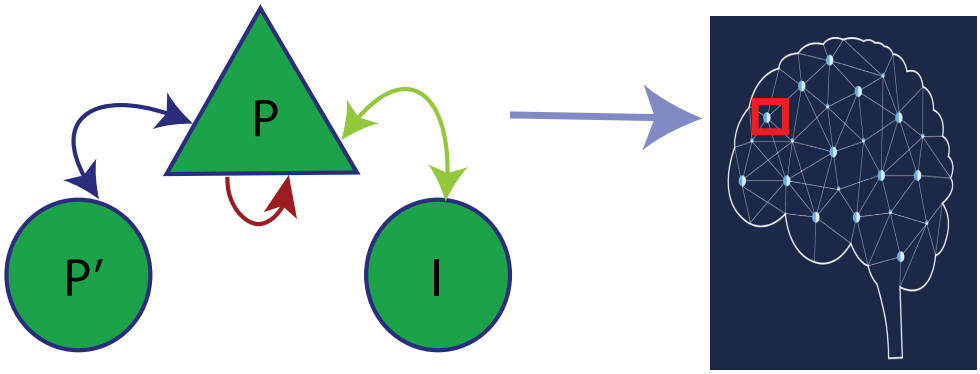

Figure 1: NMM Applications. The Left diagram: NMM interactions. The right diagram: One application of NMM to build an artificial brain.[1]

[1]The figure is taken from https://engineering.stanford.edu/magazine/article/researchers-look-fruit-fly-help-understand-human-brain/

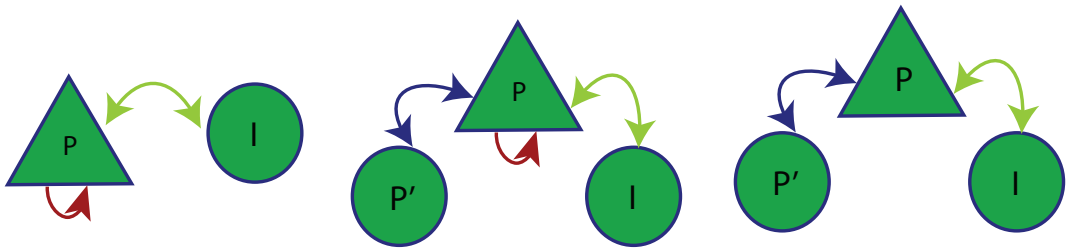

Figure 2: Interactions between neuronal populations: right diagram indirect, left diagram direct, and middle diagram double excitatory feedback. P: The main population of pyramidal neurons. I: The inhibitory interneuron population. P′: The secondary population of pyramidal neurons.

1.1 Thesis Motivations and Contributions

From the state-of-art in neural mass model analysis and applications, the proposed methods and architectures cannot analyze the model's underlying behavior over high-dimensional parameter space. In particular, bifurcation [3] only deals with low-dimensional parameter space. Moreover, to develop a method for using the neural mass model over real EEG signals, there is no single way for the use of NMMs to generate and mimic the dynamics of EEG time series.

In this thesis, starting from solutions to analyze neural mass models over low-dimensional parameter space, we develop a new method that interprets behavioral dynamics that are not interested physiologically and also the ones that might be of interest in pathological studies. The proposed solution can also be used in low-dimensional parameter space and identifies the underlying behavioral dynamics of the NMM. Moreover, we proposed a novel method that characterizes each behavior. Unlike the existing literature, the proposed method characterizes each dynamic quantitatively and identifies dynamics from generated time series. Finally, we extended our proposed method to detect transitions between dynamics over multi-dynamical simulated time series.

1.2 Thesis Layout

In chapter 2, the principal concepts and descriptions used in this thesis are introduced. In chapter 3, first, the neural mass model used in the study [3] is introduced, then the new novel algorithm to create a dictionary of behavioral dynamics over high-dimensional parameter space is developed. In chapter 4, the proposed method is illustrated to demonstrate the use of the neural mass model over real EEG data, especially in pathological cases. Finally, in chapter 5, the thesis's conclusion is provided, and the future research directions this thesis can follow are highlighted.

1.3 Publications

- Obai Bin Ka'b Ali, **Sepehr Radmannia**, Alexandre Vidal, Hassan Rivaz, Christophe Grova, Habib Benali. "A large-scale network computational model of bilaterally coupled neuron-glia masses", 25th Annual Meeting of the Organization for Human Brain Mapping (OHBM), 2019.

- **Sepehr Radmannia**, Obai Bin Ka'b Ali, Alexandre Vidal, Hassan Rivaz, Habib Benali. "Behavioral Dictionary of Generalized Neural Mass Model", 26th Annual Meeting of the Organization for Human Brain Mapping (OHBM), 2020.

- **Sepehr Radmannia**, Obai Bin Ka'b Ali, Alexandre Vidal, Hassan Rivaz, Habib Benali. "Generalized Neural Mass Model for Characterization EEG Dynamics Transition", 27th Annual Meeting of the Organization for Human Brain Mapping (OHBM), 2021.

- **Sepehr Radmannia**, Obai Bin Ka'b Ali, Alexandre Vidal, Hassan Rivaz, Habib Benali. "Characterization The Dynamics of Generalized Neural Mass Model", 27th Annual Meeting of the Organization for Human Brain Mapping (OHBM), 2021.

Chapter 2

Preliminaries and Definitions

2.1 Physiological Basics

In this section, the fundamental physiological knowledge about the brain, which is required to comprehend this thesis, is provided. Neurons are the main compartments of the brain. Neurons sending and receiving signals through the network enable us to move, feel, play and enjoy our life. The type of neurons in the brain is still an active research study. There are a variety of different neurons in communication in the brain. However, we can classify neurons into three main types as follows:

2.1.1 Sensory Neurons

Sensory neurons are the first cells detecting our interactions with the environment. For instance, sensory neurons send this information through the nervous system to be responded when we touch a hot surface.

2.1.2 Motor Neurons

Motor neurons are responsible for controlling all of our muscles by sending impulses to them.

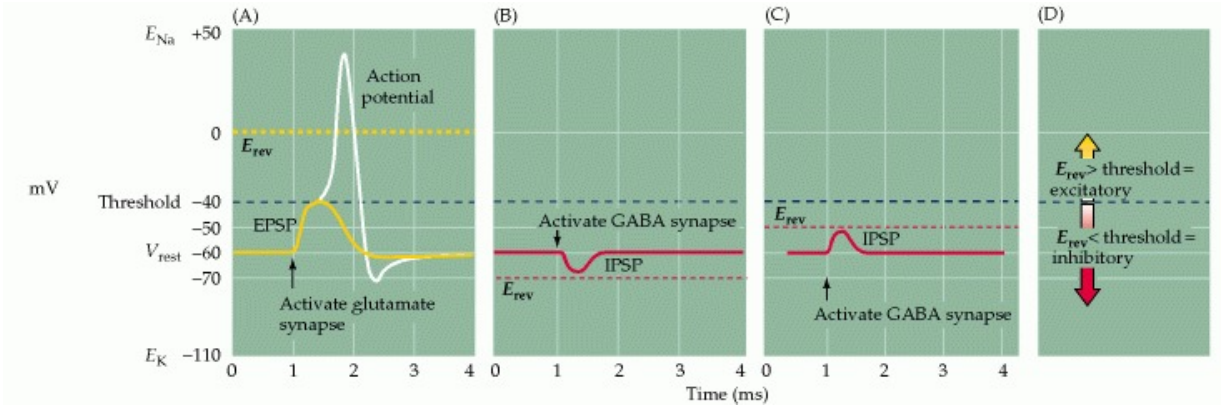

Figure 3: Reversal potentials and threshold potentials determine postsynaptic excitation and inhibition. (A) If the reversal potential for a PSP (0 mV) is more positive than the action potential threshold (-40 mV), the effect of a transmitter is excitatory, and it generates EPSPs. (B) If the reversal potential for a PSP is more negative than the action potential threshold, the transmitter is inhibitory and generate IPSPs. (C) IPSPs can nonetheless depolarize the postsynaptic cell if their reversal potential is between the resting potential and the action potential threshold. (D) The general rule of postsynaptic action is: If the reversal potential is more positive than threshold, excitation results; inhibition occurs if the reversal potential is more negative than threshold.[1]

2.1.3 Interneurons

As it is evident, interneurons connect sensory neurons to motor neurons and transfer information between these groups of neurons. They also can communicate with each other and building a more complex network of neuronal cells.

The neurotransmitter that a neuron uses is one way to identify the type of the neuron. Neurotransmitters are chemical molecules that are used by neurons for transmission messages. There are two main types of neurons based on their neurotransmitters, e.g., excitatory neurons and inhibitory neurons. As their name suggests, excitatory neurons promote the electrical response calls action potential in the adjacent neurons while inhibitory neurons prevent it see Figure 3.

[1]The figure is taken from https://www.ncbi.nlm.nih.gov/books/NBK11117/figure/A478/?report=objectonly

2.2 Computational Neuroscience History

The computational neuroscience field of study develops models to simulate the brain's dynamic. There are two modeling perspectives in these type of studies, e.g., microscopic level and macroscopic level which they are described as follows:

2.2.1 Microscopic Modeling

These computational models are at the level of the single neuron. The neurons in the brain communicate with each other by their connections, and abrupt changes over membrane potential result in sending a response to their adjacent neurons, which it calls action potential. Microscopic computational models have been developed to describe and study these electrical phenomenal at the level of single neurons. The model of Hodgkin and Huxley (1952) [4] is one example of microscopic modeling, which studied the neurons' interactions and gain knowledge about the generation of the action potential and its propagation over neuron connections.

2.2.2 Macroscopic Modeling

Macroscopic models tend to study the overall behavior of neurons. One way to investigate the function of neurons' population is to use the network of microscopic models (Brunel Wang, 2001 [5]; Wong Wang [6], 2006; Stefanescu, Jirsa, 2008 [7]). These models are computationally expensive. Therefore, other techniques developed to model the mass of neurons and allowed us to understand the organization of interactions at the level of cells. The proposed models enabled one to simulate the neuronal excitation and inhibitions and their consequences over neuronal rhythms. The developed models of the mass of neurons are called neural mass models, the neural mass models originated by the work of Beurle (1956) [8]. The neural mass model proposed we studied the activity propagation over the mass of cells by considering the active neurons' density. Griffith and the coauthors followed

the work to reproduce the excitatory and inhibitory interactions between neural cells. They introduce a second-order linear differential operation (Griffith, 1963, 1965) [9], [10]. Thereafter, the localized nonlinear temporal dynamics of the neurons over voxel are derived by Wilson and Cowan (1972, 1973) [11], [1]. Their model of two subpopulations enabled one to derive the average firing rates of the mass of neurons. Their work illustrated how differential equations could be used to model neuronal interactions, and from then it has been published several papers based on the concepts introduced by them. Several papers were published to extend their work, and they are all based on their assumptions; that's why we call all these models generalized neural mass models. In this, we have analyzed the Generalized Neural Mass Model (GNMM) introduce in [3]. The GNMMs can be validated by comparing their output with the experimental result of electroencephalography (EEG) recordings (Lopes da Silva, Hoeks, Smits, Zetterberg, 1974) [12].

2.3 Bifurcation Analysis of Co-dimension One

Bifurcation analysis is a well-known technique used in steady-state nonlinear systems to investigate underlying behavioral dynamics. Different software is implemented based on numerical analysis to investigate the steady-state system's dynamic over the system's parameters. To analyze the neural mass model introduce in [3] bifurcation is used. They have implemented methods in the MATLAB platform to derive the bifurcation diagram of the system. The definition of different bifurcation points used in this thesis are provided as follows:

2.3.1 Saddle-Node Bifurcation

The saddle-node bifurcation is when two singular points collide with each other, resulting in both of them disappear. By changing the bifurcation parameter near saddle-node two singular points, have k and $k+1$ associated real negative eigenvalues.

2.3.2 Hopf Bifurcation

Hopf bifurcation is the place when the system's singular points stability changes by a pair of purely imaginary eigenvalues Resulted in the birth of limit cycles. The bifurcation can be supercritical or subcritical, respectively. The limit cycle is either stable or unstable based on the bifurcation is supercritical or subcritical, respectively. Hopf can be located numerically by finding changes of sign in the real part of a couple of complex conjugate eigenvalues associated with a singular point [3].

2.4 Measurements

The standard approach to validating neural mass models is to compare the proposed model's output with experimental results such as Electroencephalogram (EEG) signals. In this section, we first discuss the EEG signal and then the different ways for EEG measurements.

2.4.1 Electroencephalogram

Electroencephalography (EEG) measurements are based on the electrical potential differences on the scalp. Pyramidal cells are the brain's main components that cause the potential differences over the human body's scalp. Therefore, EEG, by measuring the voltage potential in the scalp's surface, enables us to capture the pyramidal cells' activities with appropriate spatiotemporal resolution. Bipolar or unipolar electrodes can be used in the EEG measurement. In the first approach, the potential difference between a pair of electrodes and in the second approach, the electrode's potential is compared to a neutral electrode is measured see Figure 4.

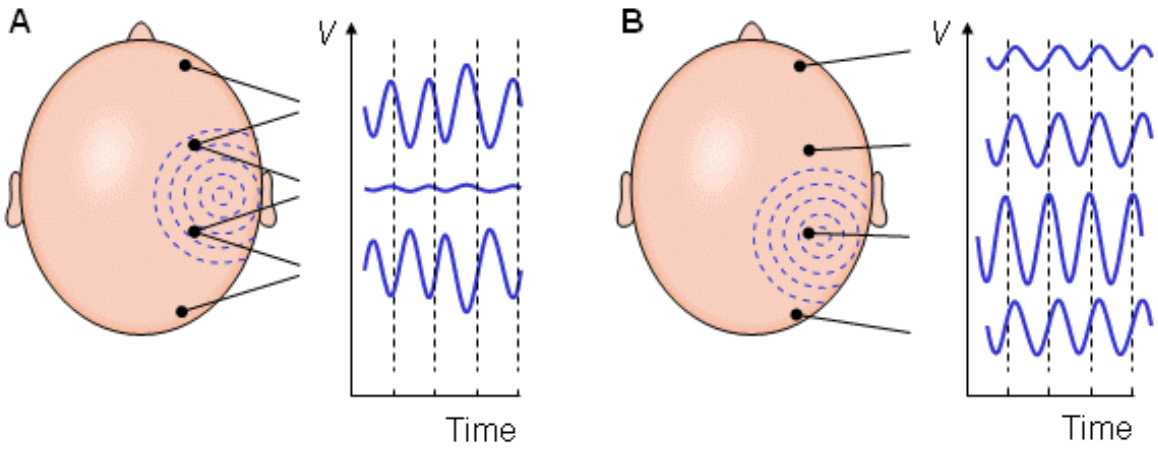

Figure 4: EEG measurement. (A) Bipolar and (B) unipolar measurements. Note that the waveform of the EEG depends on the measurement location. [2]

EEG captures neuronal activities at a time resolution of a millisecond. Spatial localization of activities is an ill-posed problem that the developed methods have to deal with the inverse problem. To better localize the source of neuronal activities, there are other techniques called Stereo Electroencephalography (SEEG). The main difference between EEG and SEEG is the place of electrodes. In SEEG, the electrodes are implanted into the brain to better localize the source of neuronal activities or seizures in patients.

[2]The figure is taken from https://www.bem.fi/book/13/13.htm

Chapter 3

Behavioral Dictionary of Generalized Neural Mass Model

The Generalized Neural Mass Analysis is proposed in this chapter [13].
Neural Mass Models (NMMs) have been used to model the neurons population's underlying behaviors on a mesoscopic scale. Variation of parameters lead to different dynamics, so finding a relation between parameter and underlying dynamics is an essential step for analyzing neural mass models. Bifurcation analysis is one of the most common techniques in order to find the underlying behavior of neuronal mass models through different parameter spaces. Nevertheless, using bifurcation analysis in high-dimensional parameter space is a challenge. Therefore, we need to modify the use of bifurcation to characterize the dynamics of NMM in high-dimensional parameter space. Here we combined classical bifurcation studies with machine learning approaches to create a behavioral dictionary of the Generalized Neural Mass Model (GNMM) in high-dimensional parameter space. We saw that besides six behaviors shown in [3], this model creates fifteen more behaviors. These 21 different behaviors are used to create a dictionary of the GNMM in high dimensional parameter space.

3.1 Overview

This section gives a brief descriptive overview of the method, and further mathematical details of the whole algorithm's steps are provided in the following sections. This method combines bifurcation analysis with a conventional classification approach to understand the behavioral dynamics of Generalized Neural Mass Models (GNMMs) over high-dimensional parameter space. The general overview of this approach is shown in Figure 5. The first step is to introduce the GNMM that we used for this analysis. This model has nine parameters that we are interested in investigating dynamical changes over the path through them. In the second step, we analyze GNMM using bifurcation according to the input considered as a bifurcation parameter. Different behavioral dynamics are considered as different classes. The third step is to classify different dynamics over the nine-dimensional parameter space. This method is performed to analyze and understand the relationship between the GNMM parameters and underlying behavioral dynamics.

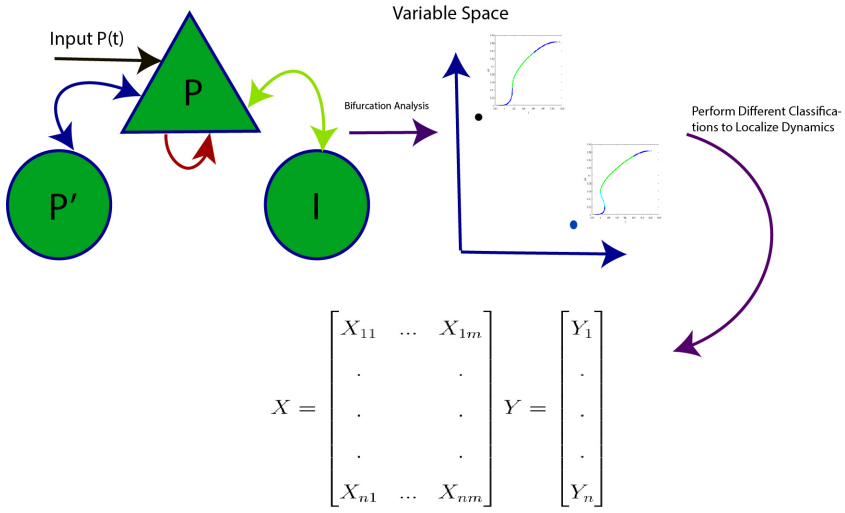

Figure 5: Hierarchical process for dynamical detection in high-dimensional parameter space. The top left picture illustrates the interactions of the used GNMM in this study. The top right image shows the transition of dynamics over variable space. 2-D axes are just for visualization. The bottom diagram is the last step that shows how we perform different classification methods to localize different dynamics over parameter space.

3.2 Generalized Neural Mass Model

In this study, the Generalized Neural Mass Model (GNMM) introduced in [3] is used. The model assumes the interaction of three neuronal populations: pyramidal neurons (main population) (P), inhibitory interneurons population (I), and secondary pyramidal neurons that are intermediary population (P′) Figure 6. The neuronal population interactions result in the activity of each population. Link from the output of the primary pyramidal Neurons (P) to their input is called direct feedback. The track which connects primary pyramidal neurons to the distant secondary pyramidal neuron's population is called indirect feedback. Both of these links result in exciting the main pyramidal neuron population. In the literature, both of these approaches exist separately. Modeling point of view cannot give any privilege to one feedback over another. Local excitatory feedback (direct link) and distant excitatory feedback (indirect link) physiologically exist. Therefore, we used the GNMM proposed in [3], in which the GNMM considers both direct and indirect excitatory feedbacks. As a result, This model contains three feedback loops on the main population (P). Two excitatory feedbacks refer to direct and indirect feedback and one inhibitory feedback from inhibitory interneuron Figure 6. Each population is characterized by:

1. Average membrane's potential transforms into an average pulse density by the neurons. This transformation is generally modeled as a sigmoid function (Freeman, 1975 [14]; Dayan ,2001 [15]; Gerstner , Kistler, 2002 [16]):

$$sigm(v) = \frac{2e_0}{1 + e^{r(v_0 - v)}}$$

   Where $2e_0$ represents the maximum discharge rate, v_0 the postsynaptic potential threshold, and r the sigmoid slope at an inflection point.

2. Average pulse density transforms into excitatory and inhibitory postsynaptic potentials. To achieving this goal, two functions have been proposed. The model that we

use in this study follows functions introduced by Van Rotterdam, Lopes da Silva, Van den Ende, Viergever, and Hermans (1982) [17]:

$$h_E(t) = Aate^{-at} h_I(t) = Bbte^{-bt}$$

Functions $h_E(.)$ and $h_I(.)$ are fundamental solutions of following F_E and F_I differential equations respectively:

$$F_E(h_E) = \frac{1}{A}(\frac{1}{a}h''_E(t)+2h'_E(t) + ah_E(t)) \tag{1a}$$

$$F_I(h_I) = \frac{1}{B}(\frac{1}{b}h''_I(t)+2h'_I(t) + bh_I(t)) \tag{1b}$$

Where A and B indicate the amplitude of postsynaptic excitatory and inhibitory potentials, respectively. $\frac{1}{a}$ and $\frac{1}{b}$ represent the time constant of excitatory and inhibitory postsynaptic potentials, respectively. Kinetics of synaptic connections and delays introduced by the circuitry of the dendritic tree (Freeman, 1975 [14]; Van Rotterdam et al [17]., 1982; Jansen et al., 1993 [18]).

Input p(t) in this GNMM model stands for the excitatory action of the distant neuronal population on the main pyramidal cell (P) through long-range synaptic connections. In this model, the input is considered as a stochastic Gaussian process Figure 6.

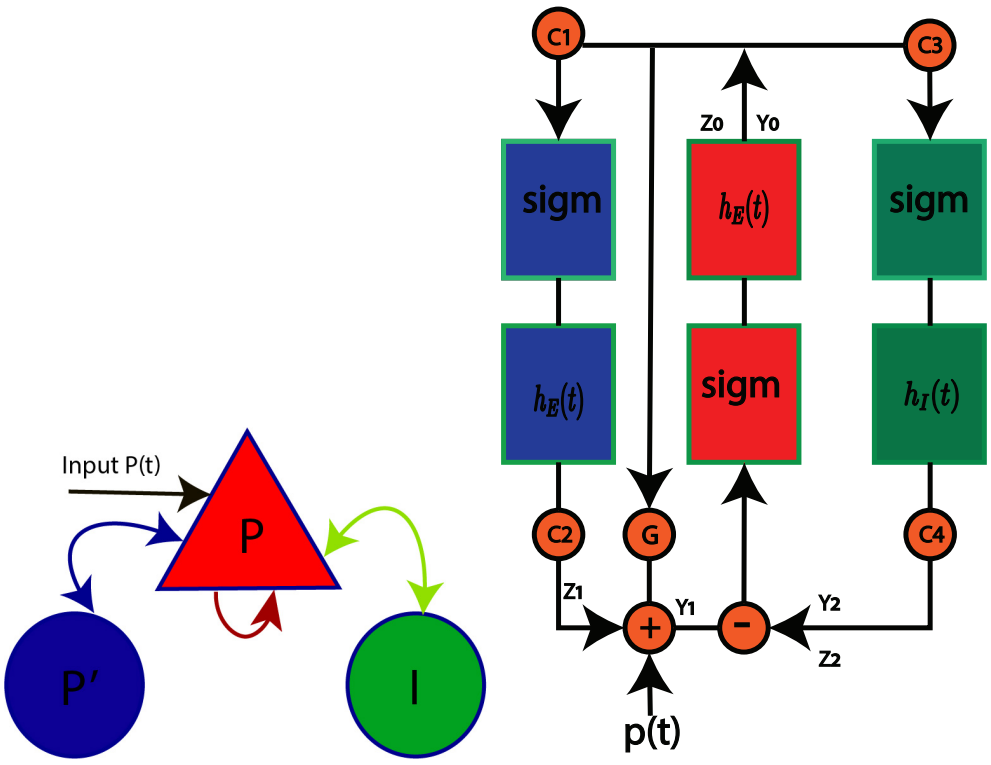

(a) Pyramidal neuron interaction schematic

(b) Neuronal population process and interaction

Figure 6: Two different views of GNMM representation. (a): Represents the interaction between the neuronal populations where P: The main population of pyramidal neurons. I: The inhibitory interneuron population. P′: The secondary population of pyramidal neurons. Blue (resp. green) arrows are excitatory (resp. inhibitory) interactions. The red arrow represents the direct feedback, and input P(t) stands for the excitatory action of the distant neuronal population. (b): Box h_E (resp. h_I): process of transforming action potentials into excitatory (resp. inhibitory) postsynaptic potential models as a second-order differential equation. Box sigm is the sigmoid function that transforms average membrane potential into average action potential density by neurons of populations P, P′, and I, respectively. C_i: $1 \leq i \leq 4$ coupling gain parameters depending on the maximum number of synaptic connections between two populations, called C. G: direct feedback coupling gain. P(t): the excitatory action of the distant neuronal population. y_0, y_1, y_2: state variables. z_0, z_1, z_2: intermediary variables.

3.2.1 Generalized Neural Mass Model Architecture

Based on the three feedback interactions' aggregation, the model will give us the output, which is comparable to electroencephalography (EEG) recording. The following set of ordinary differential equations describes the synaptic connection of the model defined in

the section 3.2:

$$z_0'' = Aa * sigm(z_1 + Gz_0 - z_2) - 2az_0' - a^2 z_0 \tag{2a}$$

$$z_1'' = AaC_2 sigm(C_1 z_0) - 2az_1' - a^2 z_1 + Aap(t) \tag{2b}$$

$$z_2'' = BbC_4 sigm(C_3 z_0) - 2bz_2' - b^2 z_2 \tag{2c}$$

To be consistent with previous models, the following state variables are considered as state variables of the GNMM. The excitatory variable called y_1 is equal to $(z_1 + Gz_0)$, the inhibitory variable called y_2 is equal to z_2, and the output of the primary pyramidal cell called y_0 is equal to z_0. This GNMM architecture proposes the state variables y_1 and y_2 as the excitatory and inhibitory inputs of the main pyramidal cell population (P). By choosing these state variables, this GNMM follows the work of Jansen-Rit. Also, it is a more general model than what they proposed. With these state variables, this model equations can be written as:

$$y_0'' = Aa * sigm(y_1 - y_2) - 2ay_0' - a^2 y_0 \tag{3a}$$

$$y_1'' = AaC_2 sigm(C_1 y_0) + AaG * sigm(y_1 - y_2) - 2ay_1' - a^2 y_1 + Aap(t) \tag{3b}$$

$$y_2'' = BbC_4 sigm(C_3 y_0) - 2by_2' - b^2 y_2 \tag{3c}$$

The first-order equations of the model are written as follows:

$$y_0' = y_3 \tag{4a}$$

$$y_1' = y_4 \tag{4b}$$

$$y_2' = y_5 \tag{4c}$$

$$y_3' = Aa * sigm(y_1 - y_2) - 2ay_0 - a^2 y_0 \tag{4d}$$

$$\begin{aligned} y_4' = {} & AaC_2 sigm(C_1 y_0) + AaG * sigm(y_1 - y_2) \\ & - 2ay_4 - a^2 y_1 + Aap(t) \end{aligned} \tag{4e}$$

$$y_5' = BbC_4 sigm(C_3 y_0) - 2by_5 - b^2 y_2 \tag{4f}$$

The average number of synapses between two populations is represented by C_i parameters, which $i \in [1, 4]$. Based on the work of Jansen and Rit (1995) [18], C_i considered as constant. It is proportional to the maximum number of synapses between populations called C.

$$\forall i \in [1, 4] C_i = \alpha_i C$$

Classically, the main output of the model approximated as generated Local Field Potential (LFP) (Jansen et al., 1993) [2]:

$$LFP(t) = y_1(t) - y_2(t)$$

A summary of each parameter interpretation is given in Table 3.

Table 3: Descriptions of The Generalized Neural Mass Model Parameters

Parameter	Description
A	Average excitatory synaptic gain
B	Average inhibitory synaptic gain
$\frac{1}{a}$	Time constant of excitatory postsynaptic potentials
$\frac{1}{b}$	Time constant of inhibitory postsynaptic potentials
e_0	Half of the maximum discharge rate of a neuronal population
v_0	Basic excitability threshold for neurons
r	Stiffness of neuronal excitability
C_1	Strength of the synaptic connections from P to P'
C_2	Strength of the synaptic connections from P' to P
C_3	Strength of the synaptic connections from P to I
C_4	Strength of the synaptic connections from I to P
C	Maximum number of synapses between populations
G	Gain of the direct excitatory feedback from P to itself

3.2.2 Bifurcation Analysis of Co-dimension Three

Bifurcation diagrams of the system for parameters C, α_2 and G by considering input p(t) as a bifurcation parameter were introduced [3]. Range and the values of the parameters for bifurcation analysis are given in Table 4. According to co-dimension one and two bifurcation analysis, it was shown that this model has five physiologically interesting dynamics over co-dimension three, which is shown below.

Table 4: Range and Value of Parameters for Co-Dimensional Three Bifurcation Analysis

Parameter	Value,Range
A	3.25 mV
B	22 mV
a	100 S^{-1}
b	50 S^{-1}
e_0	2.5 S^{-1}
v_0	6 mV
r	0.56 mV^{-1}
α_1	1
α_2	$[0, 1]$
α_3	0.25
α_4	0.25
C	$[0, 400]$
G	$[0, 80]$

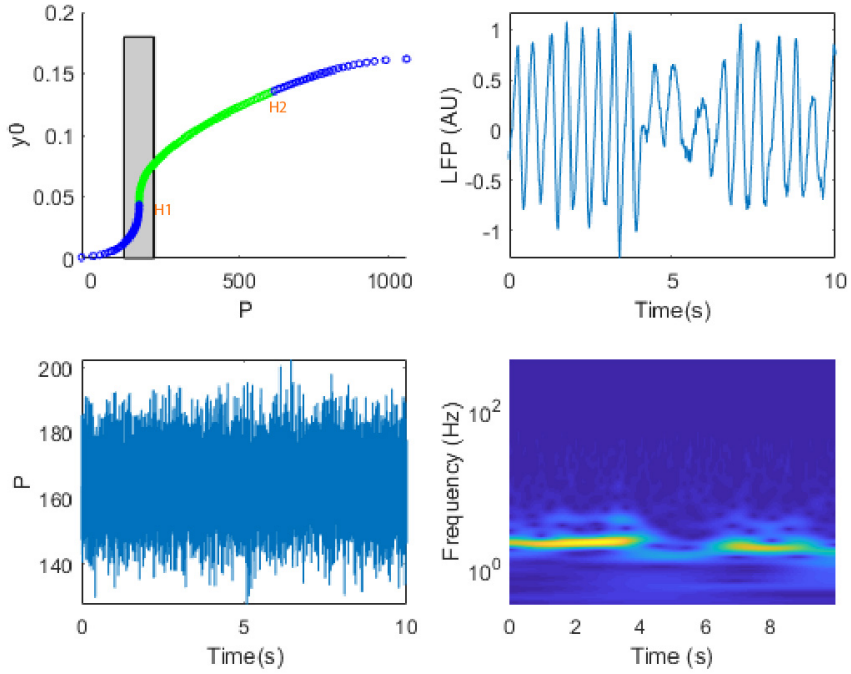

Figure 7: Bifurcation diagram considering input p as a bifurcation parameter and input distribution (left). Associated LFP time series corresponds to this bifurcation diagram and its spectrogram (right). Parameter values correspond to this bifurcation case (G = 25, α_2=0.3, and C = 130 for the simulation), called NMO. Blue curves: Stable singular points. Green curve: Singular points that four related eigenvalues have negative real parts. Red points: Supercritical Hopf bifurcations (H1 and H2). Horizontal gray bar: Confidence interval [$< p > -\delta$,$< p > +\delta$] of the Gaussian variable p(t) used to generate the time series.

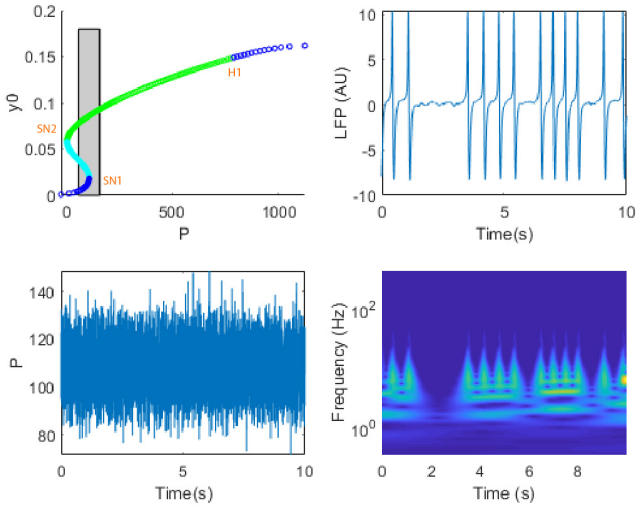

Figure 8: Bifurcation diagram considering input p as a bifurcation parameter and input distribution (left). Associated LFP time series corresponds to this bifurcation diagram and its spectrogram (right). Parameter values correspond to this bifurcation case (G = 60, α_2=0.5, and C = 150 for the simulation), called NIS. Blue curves: Stable singular points. Green and cyan curves: Singular points that four and five related eigenvalues have negative real parts. SN1 and SN2: Saddle node bifurcations. (H1): Supercritical Hopf bifurcation. Horizontal gray bar: Confidence interval [$< p > -\delta$,$< p > +\delta$] of the Gaussian variable p(t) used to generate the time series.

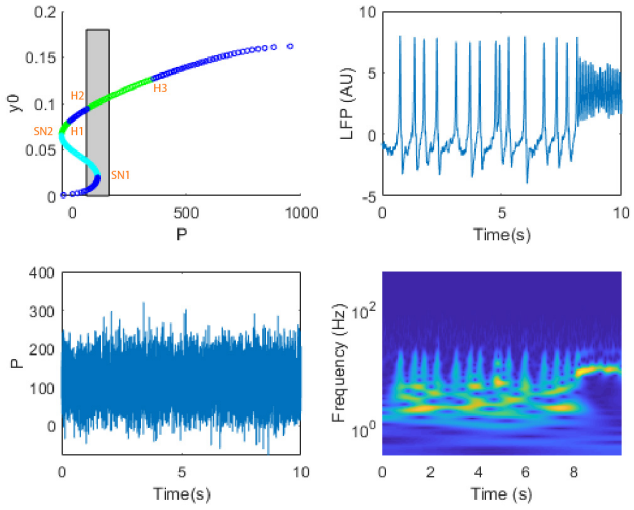

Figure 9: Bifurcation diagram considering input p as a bifurcation parameter and input distribution (left). Associated LFP time series corresponds to this bifurcation diagram and its spectrogram (right). Parameter values correspond to this bifurcation case ($G = 0$, α_2=0.8, and $C = 136$ for the simulation), called NIS-OTO. Blue curves: Stable singular points. Green and cyan curves: Singular points that four and five related eigenvalues have negative real parts. Hopf bifurcations: H1 subcritical, H2 and H3 supercritical. Saddle node bifurcations: SN1 and SN2. Horizontal gray bar: Confidence interval $[< p > -\delta, < p > +\delta]$ of the Gaussian variable p(t) used to generate the time series.

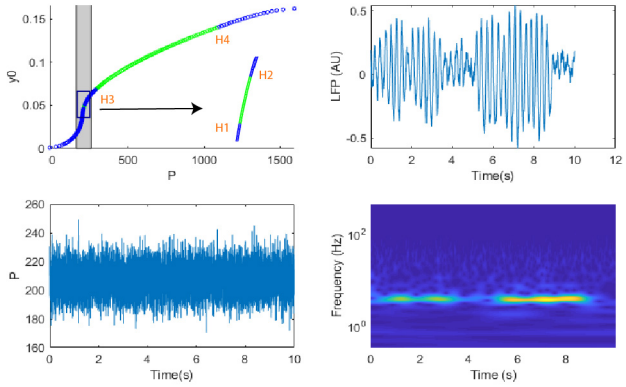

Figure 10: Bifurcation diagram considering input p as the bifurcation parameter and input distribution (left). Associated LFP time series corresponds to this bifurcation diagram and its spectrogram (right). Parameter values correspond to this bifurcation case ($G = 0$, α_2=0.3, and $C = 151$ for the simulation), called NITAM. Blue curves: Stable singular points. Green curves: Singular points that four related eigenvalues have negative real parts. Red points: Hopf bifurcations (H1, H2, and H3 subcritical and H4 supercritical). Horizontal gray bar: Confidence interval $[< p > -\delta, < p > +\delta]$ of the Gaussian variable p(t) used to generate the time series.

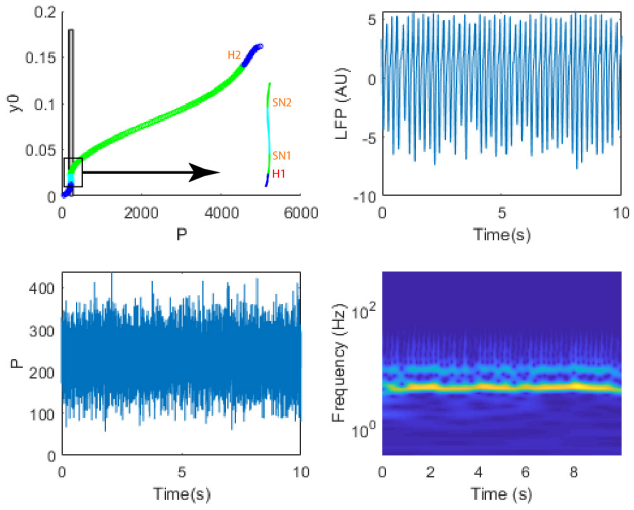

Figure 11: Bifurcation diagram considering input p as a bifurcation parameter and input distribution (left). Associated LFP time series corresponds to this bifurcation diagram and its spectrogram (right). Parameter values correspond to this bifurcation case ($G = 0$, α_2=0.3, and $C = 300$ for the simulation), called NIS-STO. Blue curves: Stable singular points. Green and cyan curves: Singular points that four and five related eigenvalues have negative real parts. Hopf bifurcation (H1 subcritical and H2 supercritical). Saddle node bifurcation (SN1 and SN2). Horizontal gray bar: Confidence interval $[< p > -\delta, < p > +\delta]$ of the Gaussian variable p(t) used to generate the time series.

3.2.3 Generalized Neural Mass Model Parameters

The NMM parameters' ranges and values are based on previous studies. Different experimental analysis has shown the range of different parameters which they are physiologically possible. The ranges of parameter values considered in this study are given in Table 5. Ranges of the parameter values are introduced in [19]. They have studied the relationship between parameters of the NMM and its main frequency without considering the underlying behavioral dynamics. They proposed a range of different parameters from the literature. The value of parameters A, B, and C has been considered debatable, and we cannot specify certain values for them. New experiments show that the values for a and b, which stand for membrane time constants, can be changed due to the uncertainty of the somatic response's dendritic time constants [20], [21]. Value of a which, a is representing the excitatory membrane time constant, varies from 25 S^{-1} to 140 S^{-1} [22], [23].

Inhibitory membrane time constant refers to b changes from 6.5 S^{-1} to 10 S^{-1} [24]. e_0 changes from 0.5 to 7.5 [25]. Values of C, α_2, and G change like what has been done in bifurcation analysis. We consider this because our final result will be consistent with bifurcation analysis. It gives us the opportunity to compare it with co-dimension-three bifurcation analysis. **Over high-dimensional parameter space, this work is the first proposed method to localize behavioral dynamics in high-dimensional parameter space**.

Parameters' ranges and values implemented for this study are given in Table 5.

Table 5: Range and Value of Parameters for The GNMM

Parameter	Value,Range
A	$[0, 10]$ mV
B	$[0, 50]$ mV
a	$[140, 25]$ S^{-1}
b	$[110, 6.5]$ S^{-1}
e_0	$[0.5, 7.5]$ S^{-1}
v_0	6 mV
r	$[0.3, 0.8]$ mV^{-1}
α_1	1
α_2	$[0, 1]$
α_3	0.25
α_4	0.25
C	$[0, 400]$
G	$[0, 80]$ mV

3.3 Proposed Method

In this section, a detection strategy for classifying dynamics in high-dimensional variable space is designed. The section is organized as follows:

First, the proposed algorithm to discriminate different behavior dynamics is presented, and different possible dynamics are illustrated; then, classification methods used for this analysis are introduced; Finally, the advantages of the proposed solution are highlighted.

3.3.1 Behavioral Dynamic Detection Strategy in High Dimension Parameter Space

This section proposed the strategy we are using to classify dynamics in high dimensional parameter space. This algorithm can be summarized by employing the following steps:

Neural Mass Modeling Dynamic Detection Algorithm

---

1. We calculate the singular point of the model depending on the input. It has been shown that we can calculate this function using the following formula [3]. This formula is calculated straightforwardly by considering all derivation equal to zero in the system of equation 4.

$$\Phi(y_0) = \frac{A}{a} sigm(\frac{A}{a}(\alpha_2 C sigm(\alpha_1 C y_0) + p) + G y_0 - \frac{B}{b}\alpha_4 C sigm(\alpha_3 C y_0), e_0, r, v_0) \quad (5)$$

2. Stability of each singular point of the model calculated by the eigenvalues of the Jacobin matrix introduced in [3]:

$$J = \begin{bmatrix} O_3 & I_3 \\ U & V \end{bmatrix}$$

Where O_3 is null matrix and I_3 is identity matrix.

$$U = \begin{bmatrix} -a^2 & \Theta & -\Theta \\ Aa\alpha_1\alpha_2 C^2 S(\alpha_1 C y_0) & G\Theta - a^2 & -G\Theta \\ Bb\alpha_3\alpha_4 C^2 S(\alpha_3 C y_0) & 0 & -b^2 \end{bmatrix}$$

$$V = \begin{bmatrix} -2a & 0 & 0 \\ 0 & -2a & 0 \\ 0 & 0 & -2b \end{bmatrix}$$

Where:

$$\Theta = S(y_1 - y_2)$$
$$y_1 = \frac{A}{a}(\alpha_2 C sigm(\alpha_1 C y_0) + p) + G y_0$$
$$y_2 = \frac{B}{b}\alpha_4 C sigm(\alpha_3 C y_0)$$
$$S(v) = 2e_0 r \frac{e^{r(v_0 - v)}}{(1 + e^{r(v_0 - v)})^2}$$

3. We extract the points were the number of singular points of the system changes depending on input p.

4. We find a different sequence of changes in a singular point, and each sequence corresponds to one dynamic of our model.

The detection strategy can be summarized as follows:
The same algorithm as bifurcation in co-dimension one is used as the first two steps. Instead of looking at bifurcation diagrams and bifurcation theory, we just consider the places where the number of singular points is changed. The sequence of singular point changes considers as our different dynamics.

3.3.2 Localization of Dynamics Over Parameter Space

The proposed algorithm to localize underlying behavior dynamics over parameter space is as follows:

1. To explore the parameter space the hypercube algorithm were performed.
2. We label five million points in the parameter space based on their corresponding dynamic, which we introduced in the previous session.
3. We perform different classification techniques such as Linear Discriminant Analysis (LDA), Quadratic Discriminant Analysis (QDA), Decision Tree (DT), random forest, and Support Vector Machine (SVM) to locate different dynamics and find the transitions between them.

To summarize this algorithm, we perform this algorithm two times. First by varying three parameters C, G, and α_2 and then by changing the nine variables A, a, B, b, r, e_0, α_2, C, G. The variation of three parameters of C, G, and α_2 gives us the ability to compare the results of the proposed algorithm with bifurcation which is the well-known technique to find underlying behavior dynamics of the model. We can perform bifurcation analysis in parameter spaces with dimensionality lower than three, and bifurcation can not be utilized over high dimensional parameter space. This gives us the ability to validate this algorithm in three-dimensional parameter space. Moreover, after we validate this algorithm, we perform it in 9-dimensional parameter space, and we locate all dynamics. **The proposed algorithm is the first method that has the ability to find the behavior dynamics of the model over high dimensional parameter space**.

3.4 Classification Techniques

In this section we introduced different classification algorithms that we used in this study. We used Python Sklearn packages for this study.

3.4.1 Linear and Quadratic Discriminant Analysis

Linear Discriminant Analysis (LDA) and Quadratic Discriminant Analysis (QDA) are two conventional classifiers, with linear and quadratic decision boundaries. These classifiers are well-known, and they have been used over different domains because of the following reasoning:

- Closed-form solutions
- Can be used in multiclass classification.
- Works well in practice.
- Have no hyperparameters to tune.
- Can be performed in a large data set in a reasonable time.

3.4.1.1 Mathematical Formulation

Both LDA and QDA models the prior probability of dataset $P(x|y=k)$ as a multivariate Gaussian process as follows:

$$P(x|y=k) = \frac{1}{(2\pi)^{d/2}|\Sigma_k|^{1/2}} exp\left(-\frac{1}{2}(x-\mu_k)^t\Sigma_k^{-1}(x-\mu_k)\right)$$

The posterior probability of each class $P(y=k|x)$ can be calculated by using the Bayesian rule:

$$P(y=k|x) = \frac{P(x|y=k)P(y=k)}{P(x)} = \frac{P(x|y=k)P(y=k)}{\Sigma_l P(x|y=l)P(y=l)}$$

class k is the final prediction of these approaches, which maximize the posterior class probability. more specifically for QDA approach log of the posterior probability is :

$$log(P(y=k|x)) = -\frac{1}{2}log(|\Sigma_k|) - \frac{1}{2}(x-\mu_k)^t\Sigma_k^{-1}(x-\mu_k) + log(P(y=k)) + Constant$$

Where the constant corresponds to $P(x)$ plus all other constant factors in the Gaussian distribution. The final prediction is the one that maximizes the above log-posterior probability.

If we assume all covariance matrixes for different classes are the same, QDA becomes LDA, and log-posterior probability can be summarized as follows:

$$log(P(y = k|x)) = -\frac{1}{2}(x - \mu_k)^t \Sigma_k^{-1}(x - \mu_k) + log(P(y = k)) + Constant$$

3.4.2 Decision Tree and Random Forest

Decision Trees (DT) are a non-parametric supervised learning method. Like other classification techniques, DTs are willing to predict variables' target classes by their corresponding features. Here some advantages of DTs that are useful for our study is summarized:

- Make the visualization of data easy in high dimensional data.
- Time performance over big data is good, and it takes a reasonable time.
- It can handle multiclass classification.
- Easy to interpret, although we have to be careful about the DT depth

The DTs performing the following steps for the classification of the dataset.

1. Select the best attribute using Attribute Selection Measures (ASM) to split the records. There are two approaches for ASM which both try to measures the impurity in the dataset, so either one of them can be treated as a cost function of DTs.

   Gini index:

   $$GINI(D) = 1 - \Sigma_{i=l}^{m} P_i^2$$

   Information gain:

   $$INFO(D) = -\Sigma_{i=1}^{m} P_i log_2(P_i)$$

Where D stands for subspace of dataset that we want to split it to two purer subsets. and P_i is the probability of class i in subset D.

2. Break the dataset into a smaller subset using the best feature that makes each subset purer than the previous dataset.

3. Repeat these steps recursively until one of these criteria becomes true:

   - All the subsets on the leaf of the tree are completely pure.
   - The threshold for the depth of the DT is passed.

Considering just a single tree for the prediction can result in over-fitting. It has been shown that DT cannot give us the global solution of the cost function, and a little change of the variables can result in different partitioning of variable space. Including a large number of three instead of one overcomes this problem. Each tree in the ensemble is grown according to a random set of rules. This method is called random forest.

3.4.3 Support Vector Machine

The Support Vector Machine (SVM) algorithm aims to find a hyperplane in the feature space that classifies the data points. The SVM objective is to find a plane that maximizes the margin between two separate classes. Maximizing margins between classes may result in classification with more confidence. Hyperplanes are the decision boundaries between two classes in the SVM approach. The dimensionality of hyperplanes depending on the feature space. If feature space is N-dimensional space, hyperplane has N-1 dimensions. To be able to have a non-linear hyperplane, we have to first transfer data space to another space using a kernel function. Different kernel functions have been introduced in the literature. In this study, we are using the polynomial kernel function with degree 3. To find the best degree for the polynomial, first, we did hyper-parameter tuning.

3.5 Results

In this section, the effectiveness of the proposed method is validated against bifurcation theory. First, The results in three-dimensional parameter space are shown. The comparison with a bifurcation in co-dimension three has been made. Second, the results in 9-dimensional parameter space are represented. Third, the advantages of the introduced approach are provided.

3.5.1 Validation in Three-Dimensional Variable Space

By performing the algorithm described in section 3.3.1, nine different sequences of changes in the systems' singular point have been found Figure 12. By performing bifurcation, they have found seven different sets of behavioral dynamics. Here we found all of them, besides we saw two other sequences. These two cases are sporadic and may have been related to numerical analysis error for finding the sequences. Because they are rare, we are not considering them in our analysis. For the others, we found their corresponding bifurcation cases. Sequences are as follows:

- $[-2, 2]$: This one is related to the NMO case which has shown in Figure 7.
- $[-1, -1, 2]$: Associated sequence corresponds to the NIS case Figure 8.
- $[-2, 2, -2, 2]$: The singular points' sequence corresponds to the NITAM Figure 10.
- $[-2, 1, -1, 2]$: by taking a look over Figure 11, it is evident that this is related to the NIS-STO case.
- $[-1, -1, 2, -2, 2]$: NIS-OTO Figure 9 is the only case with five bifurcation points in which singularity changes are the same as this sequence. As a result, this order of changes in a singular point is related to NIS-OTO.

- $[-1, 1]$: This case was also found in bifurcation, but it is not physiologically interesting. Thus parameters related to this case are not interested in our analysis.

- The Null sequence: The same as the previous case, we are not interested in how all points are stable, and there are no changes over singular points. This is called all stable.

The algorithm described in section 3.3.2 is used to localize different behaviors over parameter space Table 6.

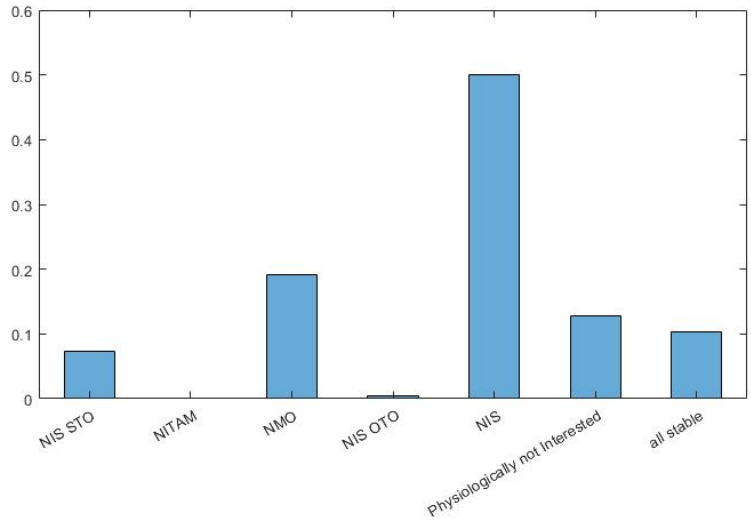

Figure 12: Distribution of different dynamics we have found over 3-dimensional parameter space. The horizontal axis represents the probability of each dynamic over the whole data space. Five-million points overall, were simulated over 3-dimensional parameter space.

Table 6: Accuracy and F1 Score Over Imbalanced Dataset

Classifications	Train Accuracy	Train F1 score	Test Accuracy	Test F1 score
LDA	84.4	52.4	84.1	52
QDA	94.4	89.2	94.2	88.7
SVM	90	90	90	90
Random-Forest	97	79.2	96.7	78.4

In order to address the imbalanced data issues, we balanced the dataset. A widely adopted and perhaps the most straightforward method for dealing with highly imbalanced

datasets is called resampling. It consists of removing samples from the majority class (under-sampling) and adding more examples from the minority class (over-sampling). We oversampled each dynamic to have a uniform distribution of each class. Then we localized dynamics Table 7.

Table 7: Accuracy and F1 Score Over Balanced Dataset

Classifications	Train Accuracy	Train F1 score	Test Accuracy	Test F1 score
LDA	70.4	70	60	45
QDA	93	92.2	90	78.7
SVM	85.5	85.4	85.5	85.3
Random-Forest	98	97	96	83

- Accuracy of random forest is related to maximum depth of the Tree. Here we used tree with depth of ten. More depth trees resulted in better accuracy but it will make interpretation harder.
- Kernel for SVM approach is considered as polynomial kernel with degree three.
- The speed performance of the SVM technique is much lower than the others. We have used ten percent of train data to train SVM.

3.5.2 Accuracy and F1 Score in Nine Dimensional Data Space

The same procedure as in three-dimensional space in eleven-dimensional space resulted in finding 21 different behavioral dynamics Figure 13. These dynamics consist of the same seven dynamics we had in three-dimensional space plus fourteen more dynamics. The algorithm described in section 3.3.2 is used to localize different behaviors over nine-dimensional parameter space Table 8.

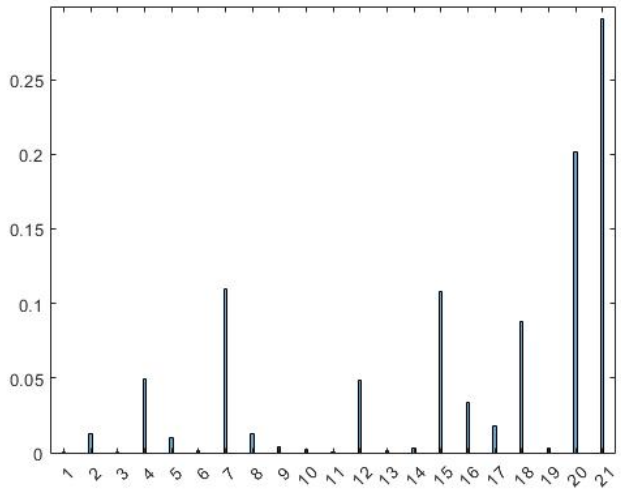

Figure 13: Distribution of different dynamics we have found over 9-dimensional parameter space. The horizontal axis represents the probability of each dynamic over the whole parameter space. Five-million points overall, were simulated over 9-dimensional parameter space.

In order to address the imbalanced data issues, we balanced the dataset. A widely adopted and perhaps the most straightforward method for dealing with highly imbalanced datasets is called resampling. It consists of removing samples from the majority class (under-sampling) and adding more examples from the minority class (over-sampling). We oversample each dynamic to have a uniform distribution of each classes.

Table 8: Accuracy and F1 Score Over Balanced Dataset

Classifications	Train Accuracy	Train F1 score	Test Accuracy	Test F1 score
LDA	59.1	58.6	58.9	58.4
QDA	71	70	70.5	70
SVM	56	54	55.5	54
Random-Forest	61	60	59	58

3.5.3 Discussion

The main power and advantages of the proposed method, in terms of model analysis, the variable of interest, and region of interest, can be summarized as follows:

- Model analysis: The represented method ensures the detection of the same results in lower-dimensional parameter space beside it gives us the capability to find the model's underlying behavioral dynamics over parameter space, which have more than three dimensions.

- Variable of interest: There are lots of debates over the value of the input in the literature. In this method, we propose to have an input value over singularity changes. Thus, this algorithm can be used to find the best value as the input of the model.

- Region of interest: Contrary to the literature, which mostly model parameters chosen over previous studies, here we have the opportunity to find the regions which are not physiologically interested. Localizing these parameter space, allow us to find the region of interest for the model.

Chapter 4

Characterization the Dynamics of Generalized Neural Mass Model

The dynamic characteristics of the GNMM is proposed in this chapter [26].
Bifurcation analysis is a classic approach for analysis underlying behavioral dynamics of NMM over the parameter space. The algorithm introduced in chapter 3 is a new way to find behavioral dynamics over high dimensional variable space compared to bifurcation, which is utilizable only in parameter space with the dimensionality of less than three. One advantage of bifurcation over this approach is bifurcation give us qualitative information about the generated time series. In this section, we proposed a method that characterizes each behavior find in [3] quantitatively. We characterize each behavior in the frequency domain. Different feature extraction methods were used in the frequency domain. First, we showed that our result is consistent with bifurcation analysis. Wavelet time decomposition is used as a feature extraction method. By training SVM using our features, we developed an algorithm that estimates an underlying model's parameters from simulated data recordings. Moreover, we simulated multi-dynamical EEG time series. By localizing transition of predicted labels from SVM, we developed a method to detect the transition time between dynamics over simulated multi-dynamical time series. This method allows us to localize changes of EEG signal over time. Besides, the dynamic which will result in

the best fit with respect to frequency will be detected.

4.1 Overview

This section summarizes the method implemented in this chapter, and the following sections illustrate the fundamental mathematics behind this algorithm more precisely Figure 14. First, by utilizing our knowledge about the NMM underlying behavior, we found appropriate value to be used as our input. Then we simulate ten-thousand LFP signals from each dynamics founded in [3] independently. It has been shown that this model has five dynamics of interest [3], which resulted in fifty thousand generated time series overall. Feature extraction methods in the frequency domain were used to characterize each dynamic. SVM, as the last step, is trained. These steps together capable of detecting the corresponding dynamic from the generated time series. Moreover, we implement the technique which addressed the gradual changes over the Electroencephalogram (EEG) time series. Physiological activities can be interpreted as instability over parameter space of Neural Mass Model (NMM). Bifurcation theory is a well-adapted technique to find the transition of dynamics over parameter space. The progressive evolution of EEG activity in the pathological case (e.g. epileptic seizures), is supposed to be characterized by a transition of the dynamics of the NMM. First, multi-dynamic EEG time series are generated to mimic such transitions over EEG time series. Then, by modeling the evolution of labels over time, the transition between dynamics over time is localized.

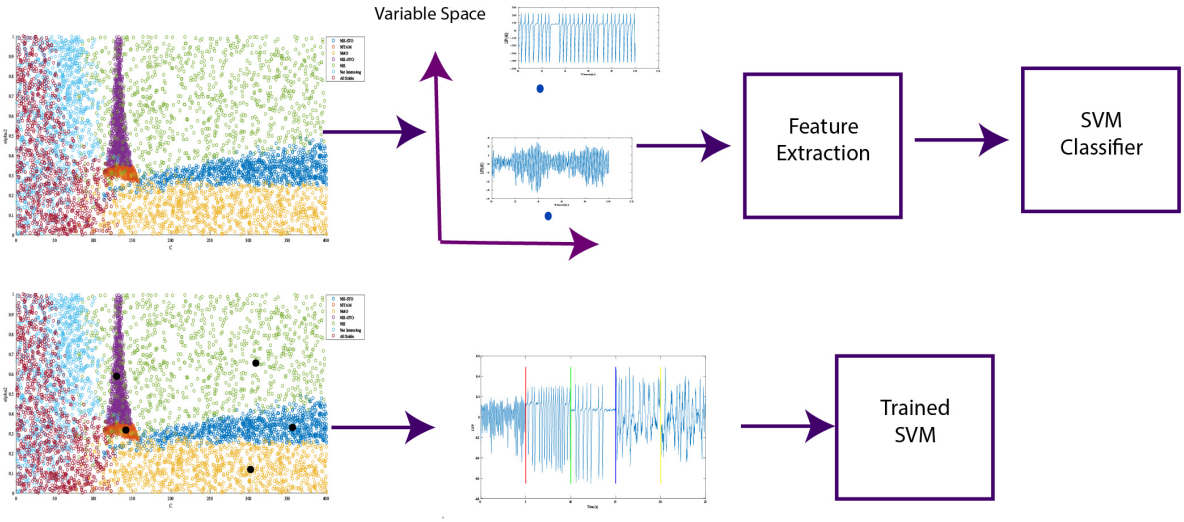

Figure 14: Hierarchical schematic for dynamic detection and transition time over three-dimensional space. 2-D axes are just for visualization. The top process illustrates the algorithm introduced to detect the corresponding dynamic from generated time series. The bottom hierarchy shows how we extended our algorithm to detect transition time between dynamics in multi-dynamical time series.

4.2 Generate Local Field Potential (LFP) Time Series

NMM used in this study is introduced in chapter 3. This study characterizes the model's behavioral dynamics over three-dimensional space where the maximum number of synaptic connections between two populations C, the direct feedback coupling gain G and α_2 are changing. The others are constant. The parameters' ranges and values are the same values used in [3] for bifurcation analysis. Each LFP time series is generated by considering input as a Gaussian process. The first positive bifurcation point is considered as the mean for Gaussian input. Two following reasoning resulted in choosing the mean value as the first positive bifurcation point:

- Neuronal dynamics have a threshold for impulsing. This threshold is the bifurcation point.

- Threshold has to be positive to have physiological meaning.

Changing STD gives us the ability to find out the model behavior over different STD values. Moreover, having a bigger STD gives the model the ability to transit between different dynamics. Input's standard deviation changes from one to one-hundred, and values were chosen for standard deviation are 2, 15, 30, 50, and 100. From each behavioral dynamics of the model that have been found in [13], we considered ten-thousand parameters to generate the LFP time series. In Figure 15, the schematic of how we generate our LFP database is shown.

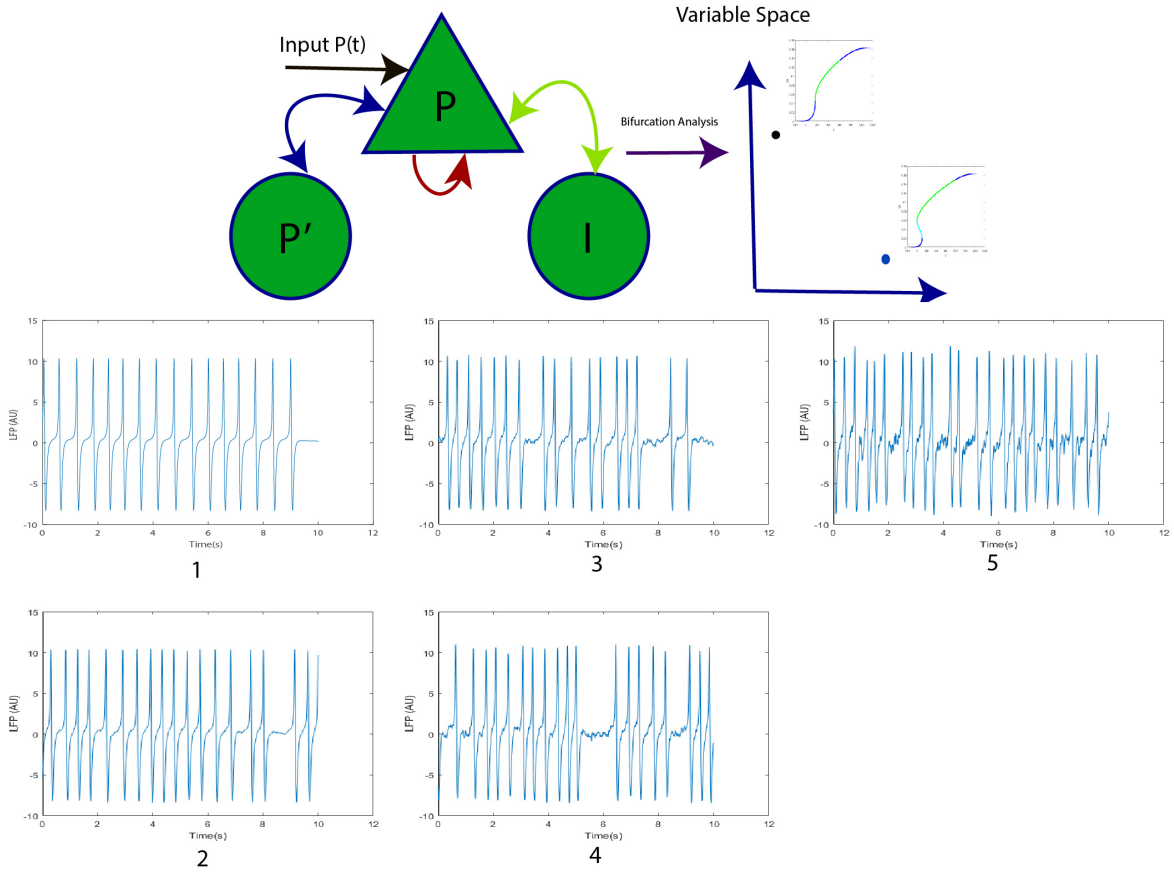

Figure 15: Hierarchical process for data generation over three-dimensional space. 2-D axes are just for visualization. The top left picture illustrates the GNMM interactions used in this study. The top right image shows the distribution of dynamics over parameter space. For each point in parameter space, we generate five LFP by changing the standard deviation of input.

4.2.1 Generate Multi-Dynamical Time Series

Multi-dynamical signals to mimic dynamics of epileptic EEG signal is generated. Each signal lasts for 25 seconds and consists of five different dynamics. Transition detection of one dynamic to another is validated by generating different sequences of transitions.

Assumption 1. *Generated dynamics are lasting at least 4 seconds. This assumption is necessary for detecting the transition time between different dynamics.*

To follow Assumption 1, our signals consist of 5 seconds of each dynamic. The NMM used in this study can generate five different behavioral dynamics. Therefore, we generated 25 seconds signal consist of all dynamics. An example of generated time series is shown in Figure 16.

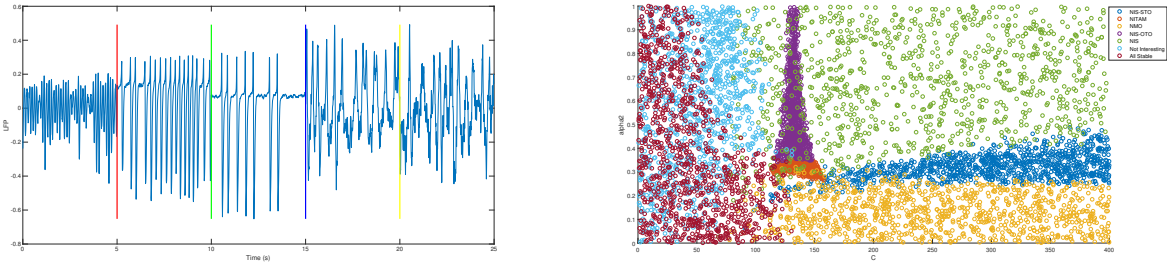

(a) Sample case of multi-dynamic signal

(b) Dynamics distribution

Figure 16: a: represents the multi-dynamic signal used in this study to mimic pathological EEG signal transition over time. Colored vertical lines show the transitions between dynamics. b: Illustrates how different dynamics are distributed over parameter space. We just used two dimensions for visualizing the dynamics even though dynamics are distributed over three-dimensional space.

Transitions between dynamics over time are made corresponding to the dynamics adjacency in variable space, So the sequence of dynamics over time is NMO, NIS-STO, NIS, NIS-OTO, NITAM. The transition of dynamics over time is just between adjacent dynamics in space.

4.3 Feature Extraction

In this section, different feature extraction methods used in our study are illustrated. First, we used Fourier analysis for feature extraction. As the Fourier analysis may contain noise, we used the welch method to decrease the effect of noise. The welch method also is a common technique used for characterizing EEG signals over different frequency bands. These two techniques are mostly revealing the central frequency of generated time series, which is not quite adequate to represent each dynamic. Moreover, we want to implement the technique to characterize real EEG signals for future works. As a result, we move to wavelet time scattering technique for feature extraction. This method indicates frequency bands of generated signals and finds temporal frequency changes over time, and makes each behavioral dynamic distinguishable.

4.3.1 Fourier Analysis

Fourier analysis represents general functions by an approximate sum of simple basis functions that in Fourier, the basic functions are sine and cosine. In this study, a Fourier is used to characterize the central frequency of the generated signal.

4.3.2 Welch Analysis

Welch's method is an approach for spectral density estimation. By splitting the signal into smaller time intervals, Welch's method improves the estimated power spectrum in terms of Signal-to-Noise Ratio (SNR), but this improvement costs as reducing the frequency resolution. The noise reduction from Welch's method is made this approach desired technique for characterizing EEG signals in frequency bands. In this study, Welch's technique is used for estimating the power of the generated signal at the main frequency.

4.3.3 Wavelet Time Scattering

The wavelet time scattering is a built-in framework of the MATLAB. The primary use of this framework is to drive features of generated one-dimensional or two-dimensional signals. By knowing the deep learning approach's advantages, this algorithm follows the same rules with some modifications. The modifications are that scattering wavelet transform uses the pre-defined filters instead of learning them. This platform combines wavelet transform with hierarchical deep learning structure to transform data to feature space, which maximizes between-class differences by preserving within-class similarity. The final features are insensitive to translations of the input on an invariance scale.

The data processing procedure in wavelet scattering is by a hierarchical structure. The output of the first level becomes the input of the next level. The input in our case is generated time series of the model. By convolving scalogram coefficients with the scaling function, The scattering coefficients are defined. The hierarchical algorithm of this feature selection method is given as follows:

- Calculate the input's wavelet coefficient with wavelet filters in the first filter bank.
- Determine the scalogram from generated data from step one
- Calculate the average for each of the modules with the scaling filter.

Repeat the process at every node.

4.4 Dynamics Characterization

In this section, we characterized each dynamic using the Welch's method. To characterize each dynamic, Fourier analysis is used as the first technique. The Welch technique has the same concept as the Fourier, but it also considers the effect of noise, and it is a better method for decreasing noise in the generated signal. The final results of both techniques are similar. Here we illustrate the Welch's results.

4.4.1 Characterization of Dynamics Using Welch's Method

The proposed algorithm to characterize underlying behavior dynamics over parameter space is as follows:

Neural Mass Modeling Characterization of Dynamics Algorithm

---

1. To extract frequency features, the welch's algorithm was performed.
2. The peak to peak difference of the signal in time-space is considered as the amplitude of the signal.
3. Each signal is characterized by two features, first the peak frequency and second the amplitude.

The following results were acquired by performing the algorithm described above.

4.4.1.1 Characteristics of NMO Dynamic

By gaining knowledge from bifurcation analysis, The qualitative information about generated time series for the NMO case is as follows:
The system's singular point is stable for $p < pH1$ and $p > pH2$ and unstable otherwise Figure 17. Considering the Gaussian variable as the input. The input variation over time results in oscillatory time series when $pH1 < p(t) < pH2$. The input value modulates oscillation amplitude and frequency.

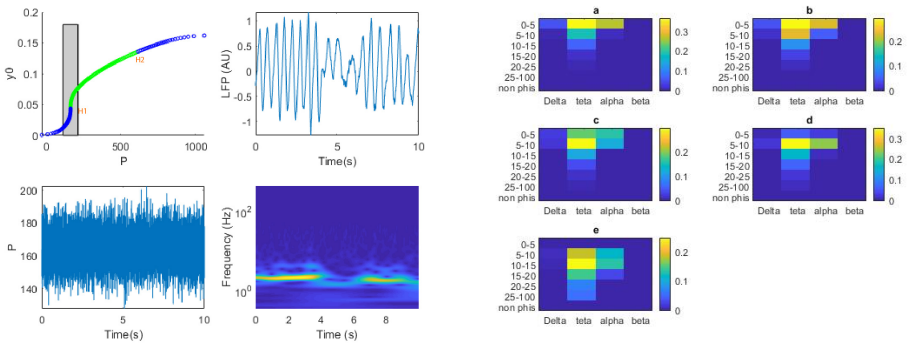

(a) Sample case of NMO dynamic (b) Characteristics of NMO dynamic

Figure 17: (a) Describes bifurcation diagram considering input p as a bifurcation parameter and input distribution (left). Associated LFP time series corresponds to this bifurcation diagram and its spectrogram (right). Parameter values correspond to this bifurcation case ($G = 25$, α_2=0.3, and $C = 130$ for the simulation), called NMO. Blue curves: Stable singular points. Green curve: Singular points that four related eigenvalues have negative real parts. Red points: Supercritical Hopf bifurcations (H1 and H2). Horizontal gray bar: Confidence interval $[< p > -\delta, < p > +\delta]$ of the Gaussian variable p(t) used to generate the time series. (b) Characteristics of the NMO dynamic over whole parameter space. a: STD of the input is 1. b: STD of input is 15. c: STD of input is 30. d: STD of input is 50. e: STD of input is 100. The main frequency over the whole parameter space remains constant even by changing the STD of input. Higher STD results in having higher amplitude.

4.4.1.2 Characteristics of NIS Dynamic

The S-shaped curve of singular points is split into three branches by two Saddle-Node SN1 and SN2. We refer to $y_0 <$ ySN1 as the lower branch, $y_0 >$ ySN2 as a higher branch, and $y_0 \in$[ySN1, ySN2], as the middle branch. Blue points in the high and low branches are stable singular points. The cyan points in the middle are unstable. Green points in the high branch are unstable. The transition between the stable state on the low branch and the high-amplitude limit cycle in the high branch occurs by choosing p(t) with an average chosen close to pSN1. As a result, the generated time series display alternations of spikes and long quiescence phases Figure 18.

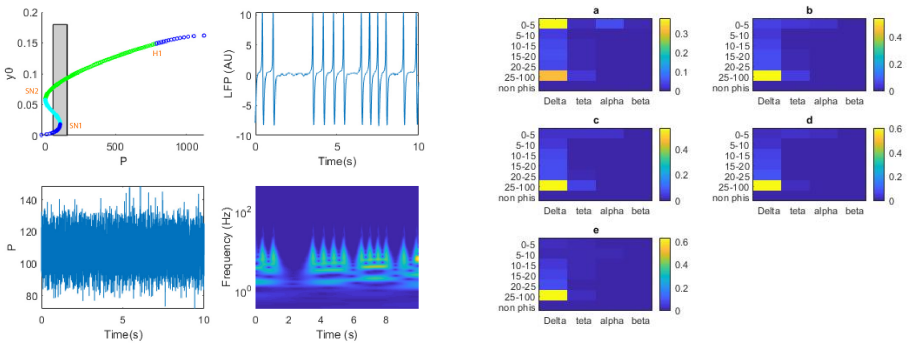

(a) Sample case of NIS dynamic (b) Characteriztics of NIS dynamic

Figure 18: (a) Bifurcation diagram considering input p as a bifurcation parameter and input distribution (left). Associated LFP time series corresponds to this bifurcation diagram and its spectrogram (right). Parameter values correspond to this bifurcation case (G = 60, α_2=0.5, and C = 150 for the simulation), called NIS. Blue curves: Stable singular points. Green and Cyan curves: Singular points that four and five related eigenvalues have negative real parts. SN1 and SN2: Saddle node bifurcations. (H1): Supercritical Hopf bifurcation. Horizontal gray bar: Confidence interval [$< p > -\delta$,$< p > +\delta$] of the Gaussian variable p(t) used to generate the time series. (b) Characteristics of the NIS dynamic over whole parameter space. a: STD of the input is 1. b: STD of input is 15. c: STD of input is 30. d: STD of input is 50. e: STD of input is 100. The main frequency over the whole parameter space remains constant even by changing the STD of input. For STD 1, the system may stay in the stable mode because of low STD, which resulted in having low amplitude signals.

4.4.1.3 Characteristics of NIS-OTO Dynamic

The singular point curve is split into three branches called low, middle, and high like NIS case. Blue points in the high and low branches are stable singular points. The cyan points in the middle are unstable. Green points in the high branch are unstable. Choosing input p(t), which varies over time, transition between high-amplitude oscillations (for p(t)$\in$[pH1, pH2], low-amplitude oscillations for p(t)$\in$[pH2, pH3] and quiescence phases for p(t)$<$pH2 may occur in generated time series. Figure 19.

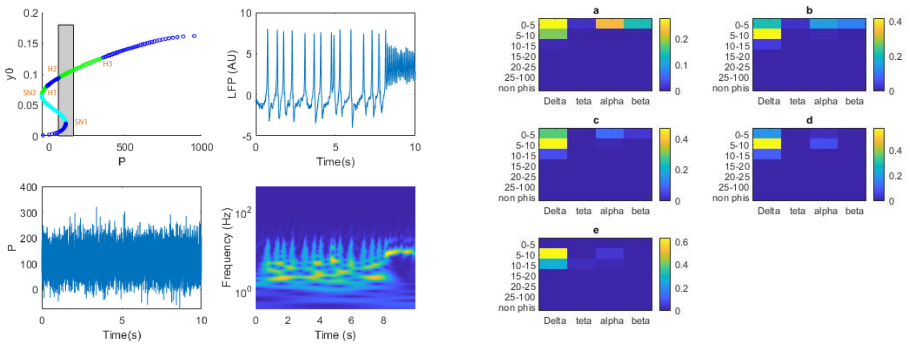

(a) Sample case of NIS-OTO dynamic (b) Characteriztics of NIS-OTO dynamic

Figure 19: (a) Bifurcation diagram considering input p as a bifurcation parameter and input distribution (left). Associated LFP time series corresponds to this bifurcation diagram and its spectrogram (right). Parameter values correspond to this bifurcation case ($G = 0$, α_2=0.8, and $C = 136$ for the simulation), called NIS-OTO. Blue curves: Stable singular points. Green and Cyan curves: Singular points that four and five related eigenvalues have negative real parts. Hopf bifurcations: H1 subcritical, H2 and, H3 supercritical. Saddle node bifurcations: SN1 and SN2. Horizontal gray bar: Confidence interval $[< p > -\delta, < p > +\delta]$ of the Gaussian variable p(t) used to generate the time series. (b) Characteristics of the NIS-OTO dynamic over whole parameter space. a: STD of the input is 1. b: STD of input is 15. c: STD of input is 30. d: STD of input is 50. e: STD of input is 100. The main frequency over the whole parameter space remains constant even by changing the STD of input. We found two frequency bands that are in line with bifurcation analysis. Welch's method extracts the frequency which has the highest energy, which is resulted in having one frequency band stable than the other one.

4.4.1.4 Characteristics of NITAM Dynamic

For each value of p, the system admits a unique singular point Figure 20. Values of input p in intervals [pH1, pH2] and [pH3, pH4] admits unstable singular points (green) and stable (blue) alternatively. By choosing p(t) varying over two intervals [pH1, pH2] and [pH3, pH4], the transition between low and high-amplitude oscillations occurs in the generated time series, respectively. Quiescence phases can also appear when input p follows the stable points at lower branch Figure 20.

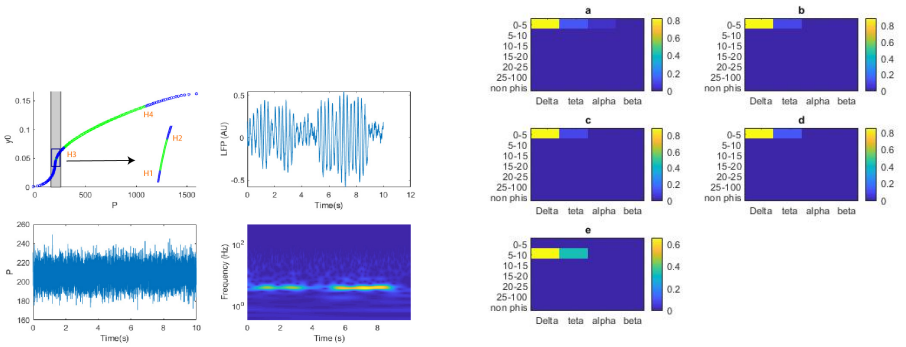

(a) Sample case of NITAM dynamic (b) Characteriztics of NITAM dynamic

Figure 20: (a) Bifurcation diagram considering input p as a bifurcation parameter and input distribution (left). Associated LFP time series corresponds to this bifurcation diagram and its spectrogram (right). Parameter values correspond to this bifurcation case ($G = 0$, α_2=0.3, and $C = 151$ for the simulation), called NITAM. Blue curves: Stable singular points. Green curves: Singular points that four related eigenvalues have negative real parts. Red points: Hopf bifurcations (H1, H2, and H3 subcritical and H4 supercritical). Horizontal gray bar: Confidence interval $[< p > -\delta, < p > +\delta]$ of the Gaussian variable p(t) used to generate the time series (b) Characteristics of the NITAM dynamic over whole parameter space. a: STD of the input is 1. b: STD of input is 15. c: STD of input is 30. d: STD of input is 50. e: STD of input is 100. The main frequency over the whole parameter space remains constant even by changing the STD of input. For Lower STD, the dynamic reveals just one frequency. The reason for this is that the input follows the orbit in the first interval. Once we increase input STD, it also explores second interval results in having two frequency bands. Welch's method extracts the frequency with the highest energy, resulting in having one frequency band stable than the other one.

4.4.1.5 Characteristics of NIS-STO Dynamic

The singular point curve is split into three branches called low, middle, and high by two saddle-node bifurcations SN1 and SN2, as in the NIS case. The singular points of the middle branch are unstable (cyan) for p < pH1, singular points of the low branch is stable (blue) and unstable (green) alternatively, for p < pH2, the points of the high branch are unstable (green) and stable (blue) alternatively. For a Gaussian input p(t) with an average close to pH1, large oscillations, quiescence phases reflecting the input noise, and subthreshold oscillations occur as the transition in the generated time series Figure 21.

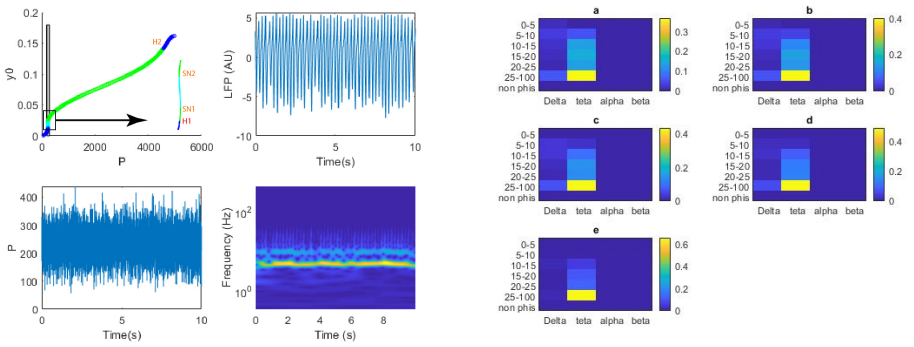

(a) Sample case of NIS-STO dynamic (b) Characteriztics of NIS-STO dynamic

Figure 21: (a) Bifurcation diagram considering input p as a bifurcation parameter and input distribution (left). Associated LFP time series corresponds to this bifurcation diagram and its spectrogram (right). Parameter values correspond to this bifurcation case ($G = 0$, α_2=0.3, and $C = 300$ for the simulation), called NIS-STO. Blue curves: Stable singular points. Green and cyan curves: Singular points that four and five related eigenvalues have negative real parts. Hopf bifurcation (H1 subcritical and H2 supercritical). Saddle node bifurcation (SN1 and SN2). Horizontal gray bar: Confidence interval $[< p > -\delta, < p > +\delta]$ of the Gaussian variable p(t) used to generate the time series. (b) Characteristics of the NIS-STO dynamic over whole parameter space. a: STD of the input is 1. b: STD of input is 15. c: STD of input is 30. d: STD of input is 50. e: STD of input is 100. The main frequency over the whole parameter space remains constant even by changing the STD of input. Welch's method extracts the frequency with the highest energy, resulting in having one frequency band, and it cannot detect the subthreshold oscillation at the generated time series.

4.5 Dynamics Detection and Transition Time

In this section, first, we proposed the algorithm for detecting the corresponding dynamic from generated time series. Then we illustrate how by combining this algorithm and modeling the density of predicted classes, we introduce a new algorithm that localizes the progressive evolution of EEG activity in the pathological case (e.g., epileptic seizures) over time.

The algorithm to detect dynamics from generated time series is as follows:

Neural Mass Model Dynamic Detection algorithm

---

1. Three-dimensional parameter space is explored using the hypercube algorithm.
2. We generate LFP time series following the process described in section 4.2
3. Time series were normalized. The normalized time series have amplitude one and mean zero. The importance of this step is to characterize each dynamic based on frequency features.
4. Normalized time series split in 2 seconds time interval resulted in having ten different intervals from each LFP time series.
5. MATLAB time scattering is used as the feature extraction method.
6. Features were fed to the SVM classifier.

The algorithm discussed above can characterize each dynamics in frequency space, making it a powerful technique to detect underlying dynamics from generated time series. Although, to be used in pathological real EEG data needs to be extended. The following procedure illustrates how we extend the algorithm to localize epileptic changes of EEG signal over time.

Neural Mass Model Localizing Transition Time in Pathological EEG

Transition Localization

1. We generated multi-dynamical time series following the procedure described in section 4.2.1.
2. Sliding window moves over the multi-dynamical time series.
3. Wavelet time scattering is used to extract features from each time interval.

4. Features were pass through the trained SVM classifier we have from the algorithm described for dynamic detection in section 4.5.

5. Evolution of predicted label's density over time is being modeled to detect the transition between dynamics.

The algorithm described above can detect the transition time between each pair of dynamics by modeling the density of predicted labels over time.

4.6 Results

The results provided in this section is first to validate the dynamic detection strategy introduced in section 4.5. Furthermore, we delivered results that show how we proceed through detecting the transition time over pathological EEG data by the extended algorithm described in section 4.5

4.6.1 Dynamic Detection Accuracy

Based on the qualitative analysis of the model that bifurcation has provided us, we proposed that systems frequency features stability over each dynamic as the hypothesis. We showed even we train the SVM classifier by using just one generated signal from each dynamic, we can get over seventy percent accuracy over the test dataset. The method's accuracy indicates that the signal frequency features will not change over one dynamics. Because of the dependency on the generated signals at the boundary of behaviors, we have to increase the training data set to characterize each dynamic and improve SVM classifier accuracy. Train and test accuracy are shown in Figure 22.

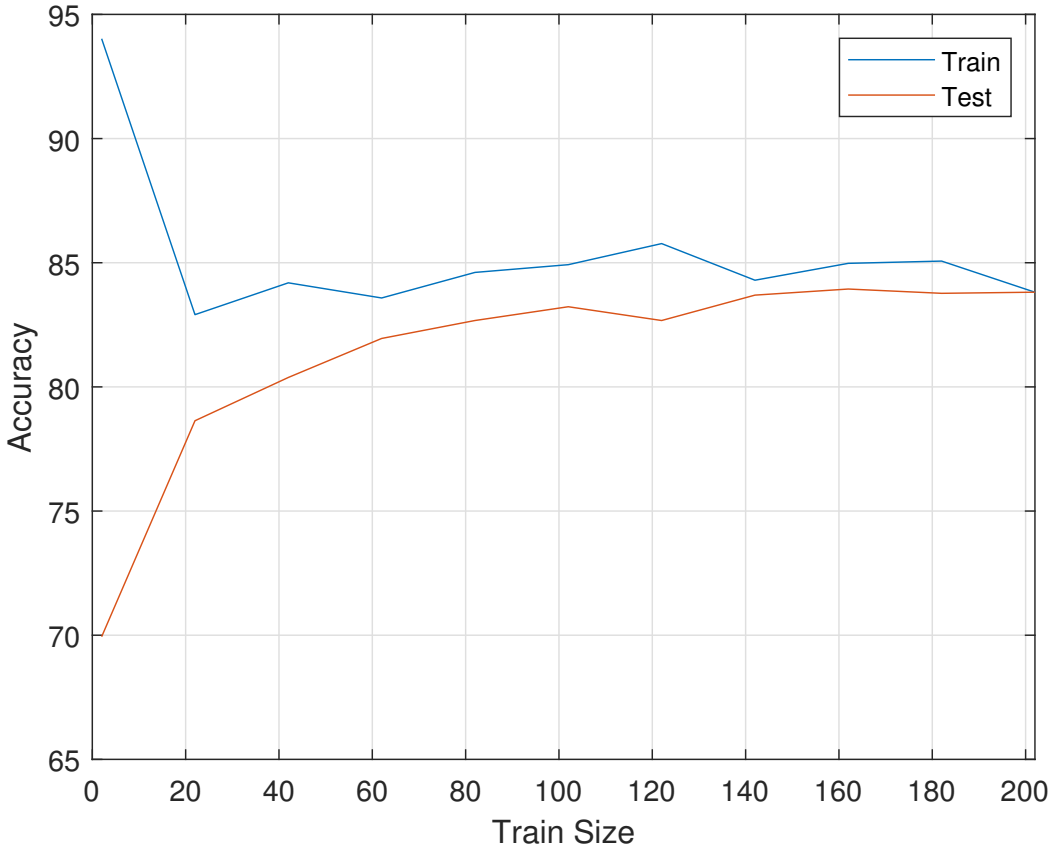

Figure 22: Train and test accuracy. The vertical axis is representing the percentage of the accuracy. The red color is for the test dataset, and the blue color is showing the training dataset. The horizontal axis shows the number of the point from each data set that is used for training.

Confusion matrix of dynamic detection algorithm introduced in section 4.5 is provided in Table 9. This matrix shows the accuracy of prediction over each dynamic separately in the test data set. Because of the unbalanced test data set to validate the proposed algorithm, a diagonalized confusion matrix has to be reported in addition to accuracy, which was provided in Figure 22.

Table 9: Confusion Matrix Over Test Dataset

		Predicted Label				
True Label		NIS-STO	NITAM	NMO	NIS-OTO	NIS
	NIS-STO	17129	1	1046	4	999
	NITAM	132	4504	747	1256	132
	NMO	361	28	17047	329	475
	NIS-OTO	98	212	173	16636	1303
	NIS	966	1	88	29	16018

4.6.2 Transition Time Accuracy

The result shown here is based on the algorithm described in section 4.5. By looking at SVM scores' evolution over time, we proposed the changes of predicted labels density at transition time, which results in changes of a sequence of labels once the sliding window is passed through one dynamic to another dynamic. The evolution of scores over time in the specific sample case of the multi-dynamical signal is shown in Figure 23.

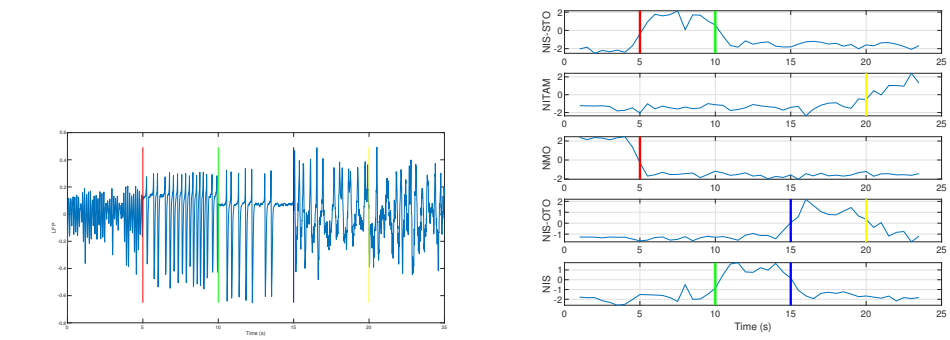

(a) Sample case of multi-dynamic signal (b) Score evolution

3 3 3 3 3 3 3 3 3 1 1 1 1 1 1 1 1 1 5 5 5 5 5 5 5 5 5 4 4 4 4 4 4 4 4 4 2 4 2 2 2 2 2 2

(c) Labels

Figure 23: (a) Represents the multi-dynamic signals used in this study to mimic pathological EEG signal transition over time. Vertical lines show the transitions between dynamics. (b) Represents the evolution of SVM scores over time. The X-axis represents the sliding window's middle time. (c) Corresponding labels of the sliding window over time. Labels 1, 2, 3, 4, and 5 correspond to NIS-STO, NITAM, NMO, NIS-OTO, and NIS, respectively.

The local changes of labels have two main reasons.

1. Misclassification of SVM approach.

2. Transitions between dynamics.

Misclassification affect the accuracy of the transition detection algorithm. Misclassified labels can result in detecting the point wrongly as the transition point, or they can result in cross the transition point without detecting it. Figure 24 describes the statistical result of the described method.

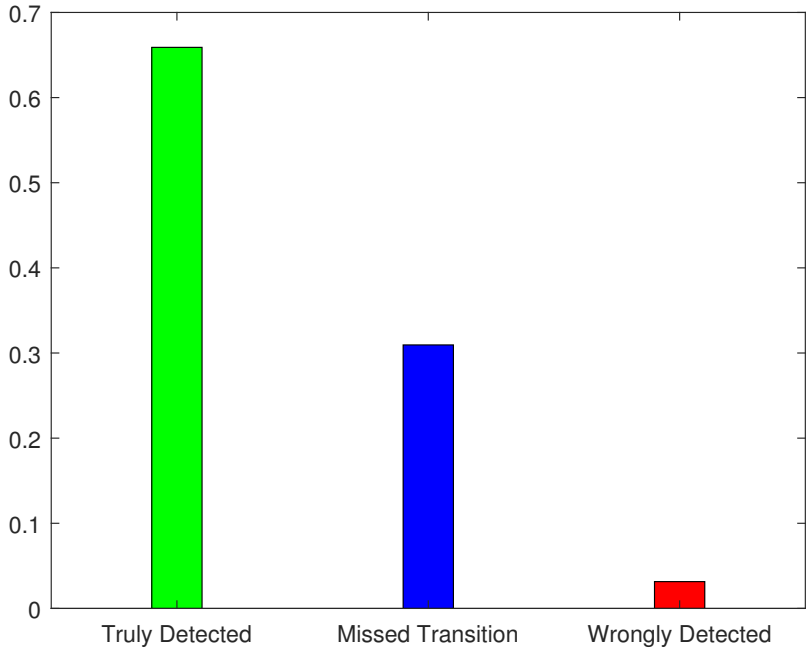

Figure 24: Accuracy of transition detection algorithm over two-thousand multi-dynamical signals.

Table 10 describes the overall accuracy of detected transition points and localization resolution of the proposed method over time.

Table 10: Accuracy and Resolution of Detected Transition Points

Accuracy	0.875
Resolution	0.56 S

Chapter 5

Conclusion and Future Work

5.1 Conclusion

This thesis addressed the problems of analyzing neural mass models besides using the neural mass model in pathological cases (e.g., epileptic seizures). The existing methods in the literature to interpret the neural mass model were explained in the introduction. The advantages and disadvantages of the methods were marked. Moreover, the fundamental hypothesizes underlying the neural mass model's use to model epileptic changes of EEG signal were discussed. According to the importance of the research study and drawbacks of existing algorithms in this domain, we first proposed a novel method to analyze the model's underlying behavioral dynamic and then introduced the new way to use the neural mass model over real pathological EEG data.

In chapter 3, bifurcation and traditional machine learning methods are combined to implement a new algorithm capable of identifying the neural mass model's underlying dynamics over high-dimensional parameter space. In comparison to bifurcation, which is capable of detecting dynamics over parameter space with dimensionality lower than three, our method can be performed over whole parameters of the neural mass model. Different machine learning methods were trained to choose the classification method which is more suitable for our problem. Finally, validation of the proposed methods was tested by

comparing it by bifurcation theory over three-dimensional variable space. The accuracy and precision of the proposed method were also reported. In high dimensional variable space, QDA gives us the best result in terms of accuracy and precision.

In chapter 4, we first characterized each dynamic of the generalized neural mass model over three-dimensional variable space to identify each dynamic from generated time series. Welch's method analysis was performed to characterize dynamics to validate each model dynamic's qualitative characteristics that bifurcation gives us. Then we used the wavelet time scattering approach to characterize each dynamic more precisely in frequency and time. The accuracy of the dynamical detection method was reported. The proposed technique was extended to be used over multi-dynamical time series where we simulate signal which mimics dynamical changes over pathological EEG cases (e.g., epileptic seizures). Finally, the accuracy and time resolution of the proposed algorithm was provided.

5.2 Future Work

Some suggestions for future research in this area are outlined below:

- In chapter 3, the algorithm to detect and localize dynamics over high dimensional parameter space is provided. However, in order to generate time series, we need to perform the co-dimension-one bifurcation analysis to found the best value of the input. The proposed method can be extended by providing a method that learns the bifurcation points' value and makes us independent from bifurcation analysis.

- The proposed technique in chapter 3 localize each dynamic over parameter space. However, the parameters that result in the model's physiologically not interesting dynamics are not determined. One way to extend this work is to perform variable analysis methods to discover which variables effectively generate physiologically not interesting dynamics.

- The proposed characterization technique in chapter 4 can be extended over higher

dimensional variable space.

- In chapter 4, we proposed a technique that characterizes each dynamic of the model. Despite this, we have not tried it in the real data. It could be one direction that this method can be validated over real pathological EEG signals.

References

[1] H. R. Wilson and J. D. Cowan, "A mathematical theory of the functional dynamics of cortical and thalamic nervous tissue," *Kybernetik*, vol. 13, no. 2, pp. 55–80, 1973.

[2] B. H. Jansen, G. Zouridakis, and M. E. Brandt, "A neurophysiologically-based mathematical model of flash visual evoked potentials," *Biological cybernetics*, vol. 68, no. 3, pp. 275–283, 1993.

[3] A. Garnier, A. Vidal, C. Huneau, and H. Benali, "A neural mass model with direct and indirect excitatory feedback loops: identification of bifurcations and temporal dynamics," *Neural computation*, vol. 27, no. 2, pp. 329–364, 2015.

[4] A. L. Hodgkin and A. F. Huxley, "A quantitative description of membrane current and its application to conduction and excitation in nerve," *The Journal of physiology*, vol. 117, no. 4, pp. 500–544, 1952.

[5] N. Brunel and X.-J. Wang, "Effects of neuromodulation in a cortical network model of object working memory dominated by recurrent inhibition," *Journal of computational neuroscience*, vol. 11, no. 1, pp. 63–85, 2001.

[6] K.-F. Wong and X.-J. Wang, "A recurrent network mechanism of time integration in perceptual decisions," *Journal of Neuroscience*, vol. 26, no. 4, pp. 1314–1328, 2006.

[7] R. A. Stefanescu and V. K. Jirsa, "A low dimensional description of globally coupled heterogeneous neural networks of excitatory and inhibitory neurons," *PLoS Comput Biol*, vol. 4, no. 11, p. e1000219, 2008.

[8] R. L. Beurle, "Properties of a mass of cells capable of regenerating pulses," *Philosophical Transactions of the Royal Society of London. Series B, Biological Sciences*, pp. 55–94, 1956.

[9] J. Griffith, "A field theory of neural nets: I: Derivation of field equations," *The bulletin of mathematical biophysics*, vol. 25, no. 1, pp. 111–120, 1963.

[10] J. S. Griffith, "A field theory of neural nets: Ii. properties of the field equations," *The Bulletin of mathematical biophysics*, vol. 27, no. 2, p. 187, 1965.

[11] H. R. Wilson and J. D. Cowan, "Excitatory and inhibitory interactions in localized populations of model neurons," *Biophysical journal*, vol. 12, no. 1, pp. 1–24, 1972.

[12] F. Lopes da Silva, A. Hoeks, H. Smits, and L. Zetterberg, "Model of brain rhythmic activity. the alpha-rhythm of the thalamus." *Kybernetik*, vol. 15, no. 1, pp. 27–37, 1974.

[13] S. Radmannia, O. Bin Ka'b Ali, A. Vidal, H. Rivaz, and H. Benali, "Behavioral dictionary of generalized neural mass model," in *26th Annual Meeting of the Organization for Human Brain Mapping*. OHBM, 2020.

[14] W. J. Freeman *et al.*, *Mass action in the nervous system*. Citeseer, 1975, vol. 2004.

[15] P. Dayan and L. F. Abbott, *Theoretical neuroscience: computational and mathematical modeling of neural systems*. Computational Neuroscience Series, 2001.

[16] W. Gerstner and W. M. Kistler, "Mathematical formulations of hebbian learning," *Biological cybernetics*, vol. 87, no. 5-6, pp. 404–415, 2002.

[17] F. L. Da Silva, A. Van Rotterdam, P. Barts, E. Van Heusden, and W. Burr, "Models of neuronal populations: the basic mechanisms of rhythmicity," in *Progress in brain research*. Elsevier, 1976, vol. 45, pp. 281–308.

[18] B. H. Jansen and V. G. Rit, "Electroencephalogram and visual evoked potential generation in a mathematical model of coupled cortical columns," *Biological cybernetics*, vol. 73, no. 4, pp. 357–366, 1995.

[19] L. A. Ferrat, M. Goodfellow, and J. R. Terry, "Classifying dynamic transitions in high dimensional neural mass models: A random forest approach," *PLoS computational biology*, vol. 14, no. 3, p. e1006009, 2018.

[20] H. Agmon-Snir and I. Segev, "Signal delay and input synchronization in passive dendritic structures," *Journal of neurophysiology*, vol. 70, no. 5, pp. 2066–2085, 1993.

[21] A. T. Gulledge, B. M. Kampa, and G. J. Stuart, "Synaptic integration in dendritic trees," *Journal of neurobiology*, vol. 64, no. 1, pp. 75–90, 2005.

[22] M. Derchansky, S. Jahromi, M. Mamani, D. Shin, A. Sik, and P. Carlen, "Transition to seizures in the isolated immature mouse hippocampus: a switch from dominant phasic inhibition to dominant phasic excitation," *The Journal of physiology*, vol. 586, no. 2, pp. 477–494, 2008.

[23] A. Kamal, A. Artola, G. Biessels, W. Gispen, and G. Ramakers, "Increased spike broadening and slow afterhyperpolarization in ca1 pyramidal cells of streptozotocin-induced diabetic rats," *Neuroscience*, vol. 118, no. 2, pp. 577–583, 2003.

[24] C. J. Wierenga, F. E. Müllner, I. Rinke, T. Keck, V. Stein, and T. Bonhoeffer, "Molecular and electrophysiological characterization of gfp-expressing ca1 interneurons in gad65-gfp mice," *PloS one*, vol. 5, no. 12, p. e15915, 2010.

[25] W. J. Freeman, "Eeg analysis gives model of neuronal template-matching mechanism for sensory search with olfactory bulb," *Biological cybernetics*, vol. 35, no. 4, pp. 221–234, 1979.

[26] S. Radmannia, O. Bin Ka'b Ali, A. Vidal, H. Rivaz, and H. Benali, "Characterization the dynamics of generalized neural mass model," in *27th Annual Meeting of the Organization for Human Brain Mapping*. OHBM, 2021.